

hypothesis may be written as follows: If a design limit of creep strain  $\delta_D$  is specified, it is predicted that the creep strain  $\delta_D$  will be reached when

$$\sum_{i=1}^k \frac{t_i}{L_i} = 1 \quad (18.78)$$

where  $t_i$  = time of exposure at the  $i$ th combination of stress level and temperature

$L_i$  = time required to produce creep strain  $\delta_D$  if entire exposure were held constant at the  $i$ th combination of stress level and temperature

Stress rupture may also be predicted by (18.78) if the  $L_i$  values correspond to stress rupture. This prediction technique gives relatively accurate results if the creep deformation is dominated by stage II steady-state creep behavior. Under other circumstances the method may yield predictions that are seriously in error.

Other cumulative creep prediction techniques that have been proposed include the time-hardening rule, the strain-hardening rule, and the life-fraction rule. The time-hardening rule is based on the assumption that the major factor governing the creep rate is the length of exposure at a given temperature and stress level, no matter what the past history of exposure has been. The strain-hardening rule is based on the assumption that the major factor governing the creep rate is the amount of prior strain, no matter what the past history of exposure has been. The life-fraction rule is a compromise between the time-hardening rule and the strain-hardening rule which accounts for influence of both time history and strain history. The life-fraction rule is probably the most accurate of these prediction techniques.

### 18.7 COMBINED CREEP AND FATIGUE

There are several important high-performance applications of current interest in which conditions persist that lead to combined creep and fatigue. For example, aircraft gas turbines and nuclear power reactors are subjected to this combination of failure modes. To make matters worse, the duty cycle in these applications might include a sequence of events including fluctuating stress levels at constant temperature, fluctuating temperature levels at constant stress, and periods during which both stress and temperature are simultaneously fluctuating. Furthermore, there is evidence to indicate that the fatigue and creep processes interact to produce a synergistic response.

It has been observed that interrupted stressing may accelerate, retard, or leave unaffected the time under stress required to produce stress rupture. The same observation has also been made with respect to creep rate. Temperature cycling at constant stress level may also produce a variety of responses, depending on material properties and the details of the temperature cycle.

No general law has been found by which cumulative creep and stress rupture response under temperature cycling at constant stress or stress cycling at constant temperature in the creep range can be accurately predicted. However, some recent progress has been made in developing life prediction techniques for combined creep and fatigue. For example, a procedure sometimes used to predict failure under combined creep and fatigue conditions for isothermal cyclic stressing is to assume that the creep behavior is controlled by the mean stress  $\sigma_m$  and that the fatigue behavior is controlled by the stress amplitude  $\sigma_a$ , with the two processes combining linearly to produce failure. This approach is similar to the development of the Goodman diagram described in Section 18.5.4 except that instead of an intercept of  $\sigma_n$  on the  $\sigma_m$  axis, as shown in Fig. 18.38, the intercept used is the *creep-limited static stress*  $\sigma_{cr}$ , as shown in Fig. 18.64. The creep-limited static stress corresponds either to the design limit on creep strain at the design life or to creep rupture at the design life, depending on which failure mode governs. The linear prediction rule then may be stated as

*Failure is predicted to occur under combined isothermal creep and fatigue if*

$$\frac{\sigma_a}{\sigma_N} + \frac{\sigma_m}{\sigma_{cr}} \geq 1 \quad (18.79)$$

An elliptic relationship is also shown in Fig. 18.64, which may be written as

*Failure is predicted to occur under combined isothermal creep and fatigue if*

$$\left(\frac{\sigma_a}{\sigma_N}\right)^2 + \left(\frac{\sigma_m}{\sigma_{cr}}\right)^2 \geq 1 \quad (18.80)$$

The linear rule is usually (but not always) conservative. In the higher-temperature portion of the creep range the elliptic relationship usually gives better agreement with data. For example, in Fig. 18.65a actual data for combined isothermal creep and fatigue tests are shown for several different

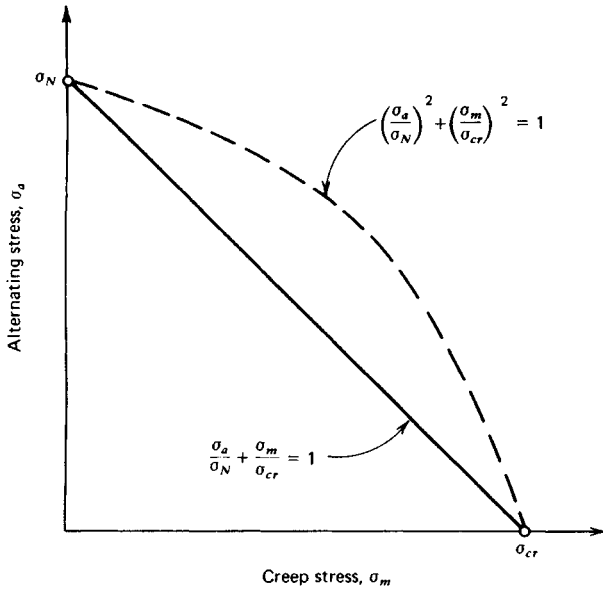


**Fig. 18.64** Failure prediction diagram for combined creep and fatigue under constant-temperature conditions.

temperatures using a cobalt-base S-816 alloy. The elliptic approximation is clearly better at higher temperatures for this alloy. Similar data are shown in Fig. 18.65*b* for 2024 aluminum alloy. Detailed studies of the relationships among creep strain, strain at rupture, mean stress, and alternating stress amplitude over a range of stresses and constant temperatures involve extensive, complex testing programs. The results of one study of this type<sup>82</sup> are shown in Fig. 18.66 for S-816 alloy at two different temperatures.

Several other empirical methods have recently been proposed for the purpose of making life predictions under more general conditions of combined creep and low-cycle fatigue. These methods include:

1. Frequency-modified stress and strain-range method.<sup>83</sup>
2. Total time to fracture versus time-of-one-cycle method.<sup>84</sup>
3. Total time to fracture versus number of cycles to fracture method.<sup>85</sup>
4. Summation of damage fractions using interspersed fatigue with creep method.<sup>86</sup>
5. Strain-range partitioning method.<sup>87</sup>

The frequency-modified strain-range approach of Coffin was developed by including frequency-dependent terms in the basic Manson–Coffin–Morrow equation, cited earlier as (18.54). The resulting equation can be expressed as

$$\Delta\epsilon = AN_f^a \nu^b + BN_f^c \nu^d \quad (18.81)$$

where the first term on the right-hand side of the equation represents the elastic component of strain range, and the second term represents the plastic component. The constants  $A$  and  $B$  are the intercepts, respectively, of the elastic and plastic strain components at  $N_f = 1$  cycle and  $\nu = 1$  cycle/min. The exponents  $a$ ,  $b$ ,  $c$ , and  $d$  are constants for a particular material at a given temperature. When the constants are experimentally evaluated, this expression provides a relationship between total strain range  $\Delta\epsilon$  and cycles to failure  $N_f$ .

The total time to fracture versus time-of-one-cycle method is based on the expression

$$t_f = \frac{N_f}{\nu} = Ct_c^k \quad (18.82)$$

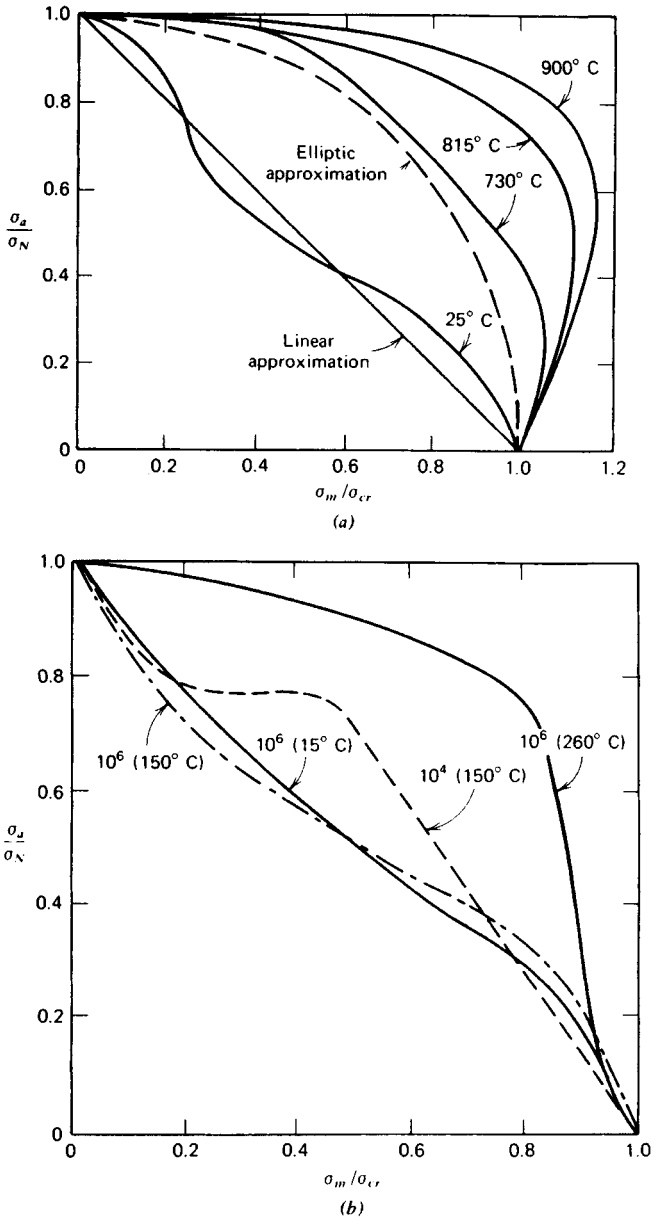


**Fig. 18.65** Combined isothermal creep and fatigue data plotted on coordinates suggested in Figure 18.64. (a) Data for S-816 alloy for 100-hr life, where  $\sigma_N$  is fatigue strength for 100-hr life and  $\sigma_{cr}$  is creep rupture stress for 100-hr life. (From Refs. 80 and 81.) (b) Data for 2024 aluminum alloy, where  $\sigma_N$  is fatigue strength for life indicated on curves and  $\sigma_{cr}$  is creep stress for corresponding time to rupture. (From Refs. 80 and 82.)

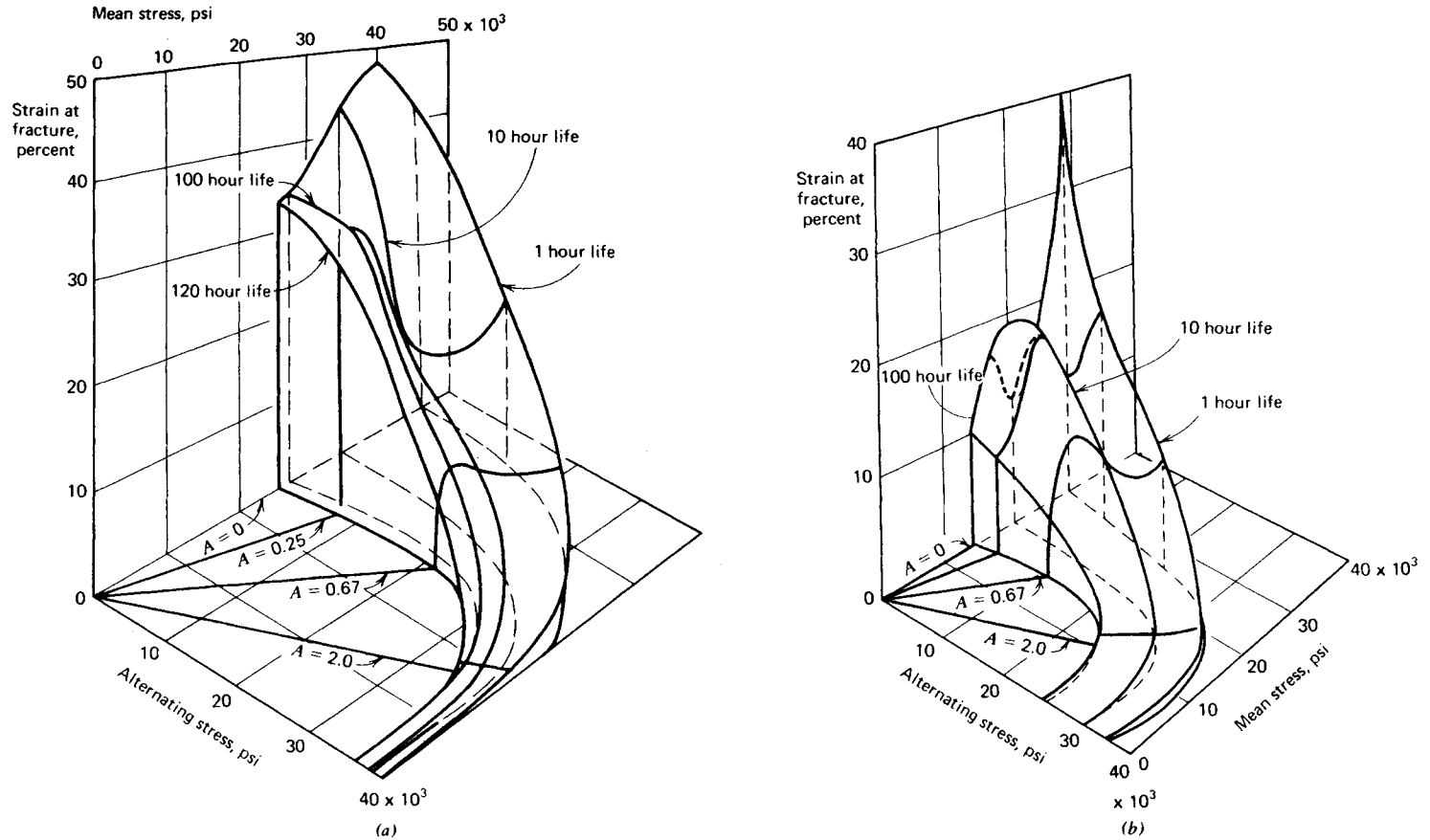


**Fig. 18.66** Strain at fracture for various combinations of mean and alternating stresses in unnotched specimens of S-816 alloy. (a) Data taken at 816°C. (b) Data taken at 900°C. (From Refs. 80 and 81.)

where  $t_f$  is the total time to fracture in minutes,  $\nu$  is frequency expressed in cycles per minute,  $N_f$  is total cycles to failure,  $t_c = 1/\nu$  is the time for one cycle in minutes, and  $C$  and  $k$  are constants for a particular material at a particular temperature for a particular total strain range.

The total time to fracture versus number-of-cycles method characterizes the fatigue-creep interaction as

$$t_f = DN_f^{-m} \tag{18.83}$$

which is identical to (18.82) if  $D = C^{1/(1-k)}$  and  $m = k/(1 - k)$ . However, it has been postulated that there are three different sets of constants  $D$  and  $m$ : one set for continuous cycling at varying strain rates, a second set for cyclic relaxation, and a third set for cyclic creep.

The interspersed fatigue and creep analysis proposed by the Metal Properties Council involves the use of a specified combined test cycle on unnotched bars. The test cycle consists of a specified period at constant tensile load followed by various numbers of fully reversed strain-controlled fatigue cycles. The specified test cycle is repeated until failure occurs. For example, in one investigation the specified combined test cycle consisted of 23 hr at constant tensile load followed by either 1.5, 2.5, 5.5, or 22.5 fully reversed strain-controlled fatigue cycles. The failure data are then plotted as fatigue damage fraction versus creep damage fraction, as illustrated in Fig. 18.67.

The fatigue damage fraction is the ratio of total number of fatigue cycles  $N'_f$  included in the combined test cycle divided by the number of fatigue cycles  $N_f$  to cause failure if no creep time were interspersed. The creep damage fraction is the ratio of total creep time  $t_{cr}$  included in the combined test cycle divided by the total creep life to failure  $t_f$  if no fatigue cycles were interspersed. A "best-fit" curve through the data provides the basis for making a graphical estimate of life under combined creep and fatigue conditions, as shown in Fig. 18.67.

The strain-range partitioning method is based on the concept that any cycle of completely reversed inelastic strain may be partitioned into the following strain-range components: completely reversed plasticity,  $\Delta\epsilon_{pp}$ ; tensile plasticity reversed by compressive creep,  $\Delta\epsilon_{pc}$ ; tensile creep reversed by compressive plasticity,  $\Delta\epsilon_{cp}$ ; and completely reversed creep,  $\Delta\epsilon_{cc}$ . The first letter of each subscript

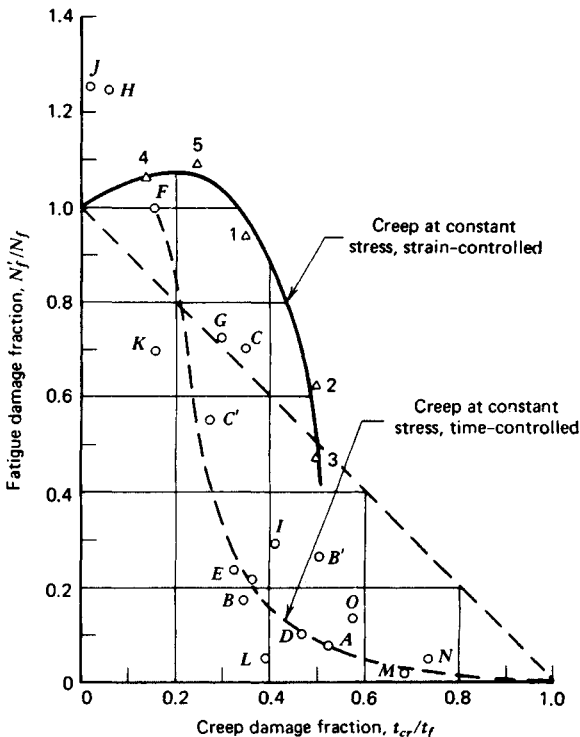


**Fig. 18.67** Plot of fatigue damage fraction versus creep damage fraction for 1 Cr-1 Mo- $\frac{1}{4}$  V rotor steel at 1000°F in air, using the method of the Metal Properties Council. (After Ref. 88, copyright Society for Experimental Stress Analysis, 1973; reprinted with permission.)

in the notation,  $c$  for creep or  $p$  for plastic deformation, refers to the type of strain imposed during the tensile portion of the cycle, and the second letter refers to the type of strain imposed during the compressive portion of the cycle. The term *plastic deformation* or *plastic flow* in this context refers to *time-independent* plastic strain that occurs by crystallographic slip within the crystal grains. The term *creep* refers to *time-dependent* plastic deformation that occurs by a combination of diffusion within the grains together with grain boundary sliding between the grains. The concept is illustrated in Fig. 18.68.

It may be noted in Fig. 18.68 that tensile inelastic strain, represented as  $\overline{AD}$  is the sum of plastic strain  $\overline{AC}$  plus creep strain  $\overline{CD}$ . Also, compressive inelastic strain  $\overline{DA}$  is the sum of plastic strain  $\overline{DB}$  plus creep strain  $\overline{BA}$ . In general,  $\overline{AC}$  will not be equal to  $\overline{DB}$ , nor will  $\overline{CD}$  be equal to  $\overline{BA}$ . However, since we are dealing with a closed hysteresis loop,  $\overline{AD}$  does equal  $\overline{DA}$ . The partitioned strain ranges are obtained in the following manner.<sup>89</sup> The completely reversed portion of the plastic strain range,  $\Delta\epsilon_{pp}$ , is the smaller of the two plastic flow components, which in Fig. 18.68 is equal to  $\overline{DB}$ . Likewise, the completely reversed portion of the creep strain range,  $\Delta\epsilon_{cc}$ , is the smaller of the two creep components, which in Fig. 18.68 is equal to  $\overline{CD}$ . As can be seen graphically, the difference between the two plastic components must be equal to the difference between the two creep components, or  $\overline{AC} - \overline{DB}$  must equal  $\overline{BA} - \overline{CD}$ . This difference then is either  $\Delta\epsilon_{pc}$  or  $\Delta\epsilon_{cp}$ , in accordance with the notation just defined. For the case illustrated in Fig. 18.68, the difference is  $\Delta\epsilon_{pc}$ , since the tensile plastic strain component is greater than the compressive plastic strain component. It follows from this discussion that the sum of the partitioned strain ranges will necessarily be equal to the total inelastic strain range, or the width of the hysteresis loop.

It is next assumed that a unique relationship exists between cyclic life to failure and each of the four strain-range components listed. Available data indicate that these relationships are of the form of the basic Manson-Coffin-Morrow expression (18.54), as indicated, for example, in Fig. 18.69 for a type 316 stainless-steel alloy at 1300°F. The governing life prediction equation, or "interaction damage rule," is then postulated to be

$$\frac{1}{N_{\text{pred}}} = \frac{F_{pp}}{N_{pp}} + \frac{F_{pc}}{N_{pc}} + \frac{F_{cp}}{N_{cp}} + \frac{F_{cc}}{N_{cc}} \quad (18.84)$$

where  $N_{\text{pred}}$  is the predicted total number of cycles to failure under the combined *straining* cycle containing all of the pertinent strain range components. The terms  $F_{pp}$ ,  $F_{pc}$ ,  $F_{cp}$ , and  $F_{cc}$  are defined as

$$\begin{aligned} F_{pp} &= \frac{\Delta\epsilon_{pp}}{\Delta\epsilon_p}, & F_{pc} &= \frac{\Delta\epsilon_{pc}}{\Delta\epsilon_p} \\ F_{cp} &= \frac{\Delta\epsilon_{cp}}{\Delta\epsilon_p}, & F_{cc} &= \frac{\Delta\epsilon_{cc}}{\Delta\epsilon_p} \end{aligned} \quad (18.85)$$

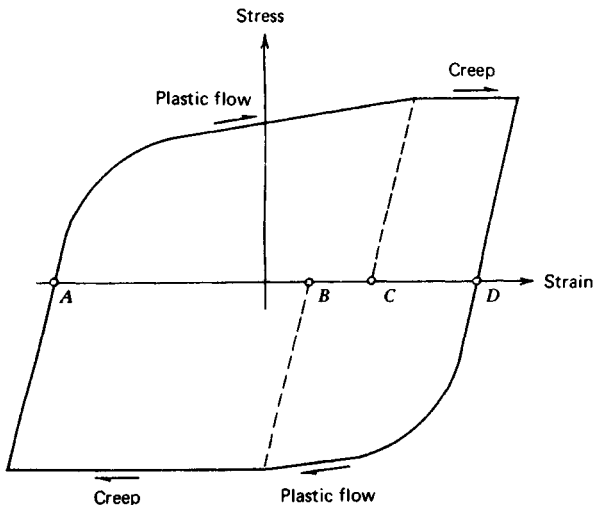


Fig. 18.68 Typical hysteresis loop.

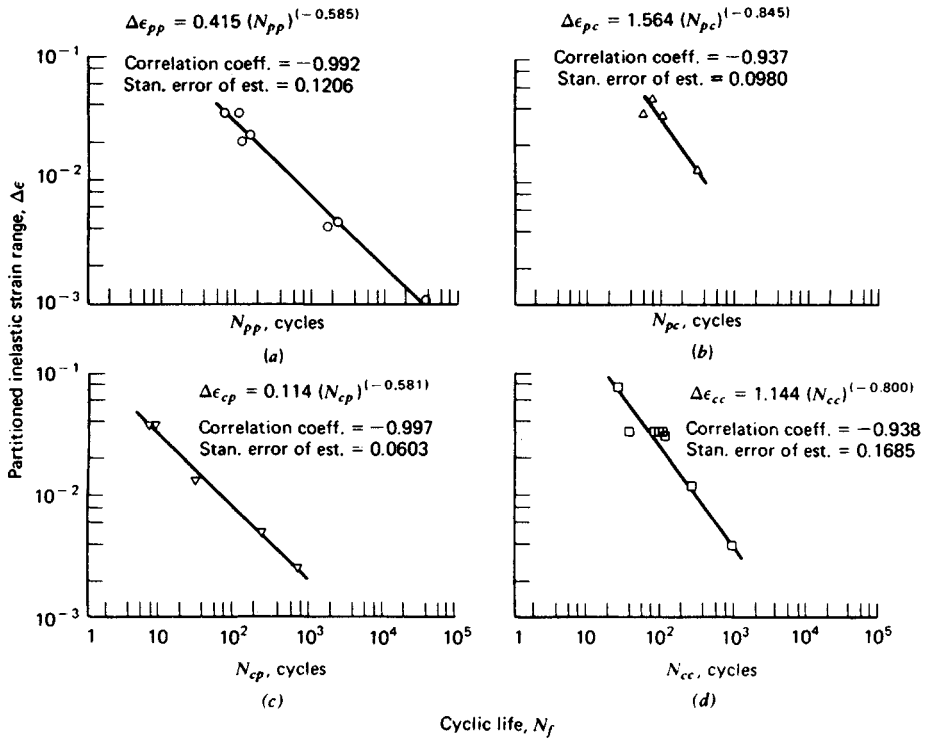


Fig. 18.69 Summary of partitioned strain-life relations for type 316 stainless steel at 1300°F (After Ref. 90): (a)  $pp$ -type strain range; (b)  $pc$ -type strain range; (c)  $cp$ -type strain range; (d)  $cc$ -type strain range.

for any selected inelastic strain range  $\Delta\epsilon_p$ , using information from a plot of experimental data such as that shown in Fig. 18.69. The partitioned failure lives  $N_{pp}$ ,  $N_{pc}$ ,  $N_{cp}$ , and  $N_{cc}$  are also obtained from Fig. 18.69. The use of (18.84) has, in several investigations,<sup>90-95</sup> shown the predicted lives to be acceptably accurate, with most experimental results falling with a scatter band of  $\pm 2N_f$  of the predicted value.

More recent investigations have indicated that improvements in predictions by the strain-range partitioning method may be achieved by using the "creep" ductility and "plastic" ductility of a material determined in the actual service environment, to "normalize" the strain versus life equations prior to using (18.85). Procedures for using the strain-range partitioning method under conditions of multiaxial loading have also been proposed<sup>94</sup> but remain to be verified more fully.

## 18.8 FRETTING AND WEAR

Fretting and wear share many common characteristics but, at the same time, are distinctly different in several ways. Basically, fretting action has, for many years, been defined as a combined mechanical and chemical action in which contacting surfaces of two solid bodies are pressed together by a normal force and are caused to execute oscillatory sliding relative motion, wherein the magnitude of normal force is great enough and the amplitude of the oscillatory sliding motion is small enough to significantly restrict the flow of fretting debris away from the originating site.<sup>96</sup> More recent definitions of fretting action have been broadened to include cases in which contacting surfaces periodically separate and then reengage, as well as cases in which the fluctuating friction-induced surface tractions produce stress fields that may ultimately result in failure. The complexities of fretting action have been discussed by numerous investigators, who have postulated the combination of many mechanical, chemical, thermal, and other phenomena that interact to produce fretting. Among the postulated phenomena are plastic deformation caused by surface asperities plowing through each other, welding and tearing of contacting asperities, shear and rupture of asperities, friction-generated subsurface shearing stresses, dislodging of particles and corrosion products at the surfaces, chemical reactions, debris accumulation and entrapment, abrasive action, microcrack initiation, and surface delamination.<sup>97-112</sup>

Damage to machine parts due to fretting action may be manifested as corrosive surface damage due to fretting corrosion, loss of proper fit or change in dimensions due to fretting wear, or accelerated fatigue failure due to fretting fatigue. Typical sites of fretting damage include interference fits; bolted, keyed, splined, and riveted joints; points of contact between wires in wire ropes and flexible shafts; friction clamps; small-amplitude-of-oscillation bearings of all kinds; contacting surfaces between the leaves of leaf springs; and all other places where the conditions of fretting persist. Thus, the efficiency and reliability of the design and operation of a wide range of mechanical systems are related to the fretting phenomenon.

Wear may be defined as the undesired cumulative change in dimensions brought about by the gradual removal of discrete particles from contacting surfaces in motion, due predominantly to mechanical action. It should be further recognized that corrosion often interacts with the wear process to change the character of the surfaces of wear particles through reaction with the environment. Wear is, in fact, not a single process but a number of different processes that may take place by themselves or in combination. It is generally accepted that there are at least five major subcategories of wear (see p. 120 of Ref. 113, see also Ref. 114), including adhesive wear, abrasive wear, corrosive wear, surface fatigue wear, and deformation wear. In addition, the categories of fretting wear and impact wear<sup>115-117</sup> have been recognized by wear specialists. Erosion and cavitation are sometimes considered to be categories of wear as well. Each of these types of wear proceeds by a distinctly different physical process and must be separately considered, although the various subcategories may combine their influence either by shifting from one mode to another during different eras in the operational lifetime of a machine or by simultaneous activity of two or more different wear modes.

### 18.8.1 Fretting Phenomena

Although fretting fatigue, fretting wear, and fretting corrosion phenomena are potential failure modes in a wide variety of mechanical systems, and much research effort has been devoted to the understanding of the fretting process, there are very few quantitative design data available, and no generally applicable design procedure has been established for predicting failure under fretting conditions. However, even though the fretting phenomenon is not fully understood, and a good general model for prediction of fretting fatigue or fretting wear has not yet been developed, significant progress has been made in establishing an understanding of fretting and the variables of importance in the fretting process. It has been suggested that there may be more than 50 variables that play some role in the fretting process.<sup>118</sup> Of these, however, there are probably only eight that are of major importance; they are:

1. The magnitude of relative motion between the fretting surfaces.
2. The magnitude and distribution of pressure between the surfaces at the fretting interface.
3. The state of stress, including magnitude, direction, and variation with respect to time in the region of the fretting surfaces.
4. The number of fretting cycles accumulated.
5. The material, and surface condition, from which each of the fretting members is fabricated.
6. Cyclic frequency of relative motion between the two members being fretted.
7. Temperature in the region of the two surfaces being fretted.
8. Atmospheric environment surrounding the surfaces being fretted.

These variables interact so that a quantitative prediction of the influence of any given variable is very dependent on all the other variables in any specific application or test. Also, the combination of variables that produce a very serious consequence in terms of fretting fatigue damage may be quite different from the combinations of variables that produce serious fretting wear damage. No general techniques yet exist for quantitatively predicting the influence of the important variables of fretting fatigue and fretting wear damage, although many special cases have been investigated. However, it has been observed that certain trends usually exist when the variables just listed are changed. For example, fretting damage tends to increase with increasing contact pressure until a nominal pressure of a few thousand pounds per square inch is reached, and further increases in pressure seem to have relatively little direct effect. The state of stress is important, especially in fretting fatigue. Fretting damage accumulates with increasing numbers of cycles at widely different rates, depending on specific operating conditions. Fretting damage is strongly influenced by the material properties of the fretting pair—surface hardness, roughness, and finish. No clear trends have been established regarding frequency effects on fretting damage, and although both temperature and atmospheric environment are important influencing factors, their influences have not been clearly established. A clear presentation of the current state of knowledge relative to these various parameters is given, however, in Ref. 109.

Fretting fatigue is fatigue damage directly attributable to fretting action. It has been suggested that premature fatigue nuclei may be generated by fretting through either abrasive pit-digging action,

asperity-contact microcrack initiation,<sup>119</sup> friction-generated cyclic stresses that lead to the formation of microcracks,<sup>120</sup> or subsurface cyclic shear stresses that lead to surface delamination in the fretting zone.<sup>112</sup> Under the abrasive pit-digging hypothesis, it is conjectured that tiny grooves or elongated pits are produced at the fretting interface by the asperities and abrasive debris particles moving under the influence of oscillatory relative motion. A pattern of tiny grooves would be produced in the fretted region with their longitudinal axes all approximately parallel and in the direction of fretting motion, as shown schematically in Fig. 18.70.

The asperity-contact microcrack initiation mechanism is postulated to proceed due to the contact force between the tip of an asperity on one surface and another asperity on the mating surface as the surfaces move back and forth. If the initial contact does not shear one or the other asperity from its base, the repeated contacts at the tips of the asperities give rise to cyclic or fatigue stresses in the region at the base of each asperity. It has been estimated<sup>105</sup> that under such conditions the region at the base of each asperity is subjected to large local stresses that probably lead to the nucleation of fatigue microcracks at these sites. As shown schematically in Fig. 18.71, it would be expected that the asperity-contact mechanism would produce an array of microcracks whose longitudinal axes would be generally perpendicular to the direction of fretting motion.

The friction-generated cyclic stress fretting hypothesis<sup>107</sup> is based on the observation that when one member is pressed against the other and caused to undergo fretting motion, the tractive friction force induces a compressive tangential stress component in a volume of material that lies ahead of the fretting motion, and a tensile tangential stress component in a volume of material that lies behind the fretting motion, as shown in Fig. 18.72*a*. When the fretting direction is reversed, the tensile and compressive regions change places. Thus, the volume of material adjacent to the contact zone is subjected to a cyclic stress that is postulated to generate a field of microcracks at these sites. Furthermore, the geometrical stress concentration associated with the clamped joint may contribute to microcrack generation at these sites.<sup>108</sup> As shown in Fig. 18.72*c*, it would be expected that the friction-generated microcrack mechanism would produce an array of microcracks whose longitudinal axes would be generally perpendicular to the direction of fretting motion. These cracks would lie in a region adjacent to the fretting contact zone.

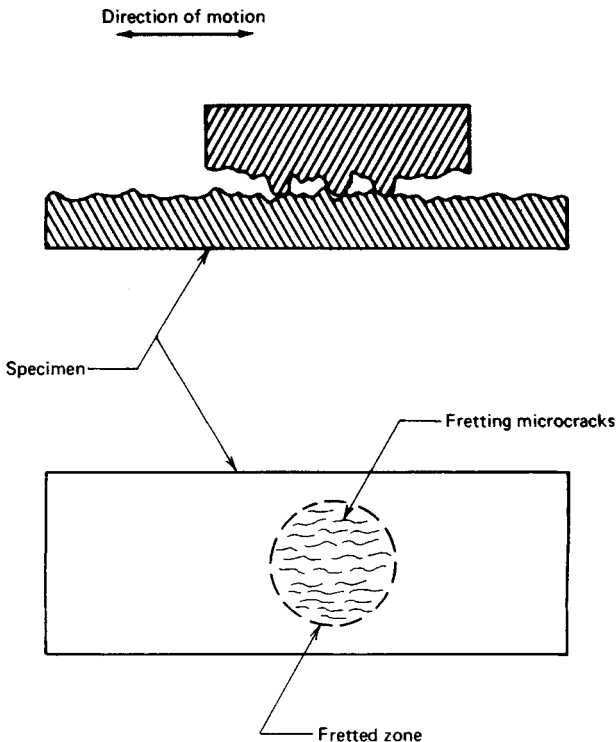


**Fig. 18.70** Idealized schematic illustration of the stress concentrations produced by the abrasive pit-digging mechanism.

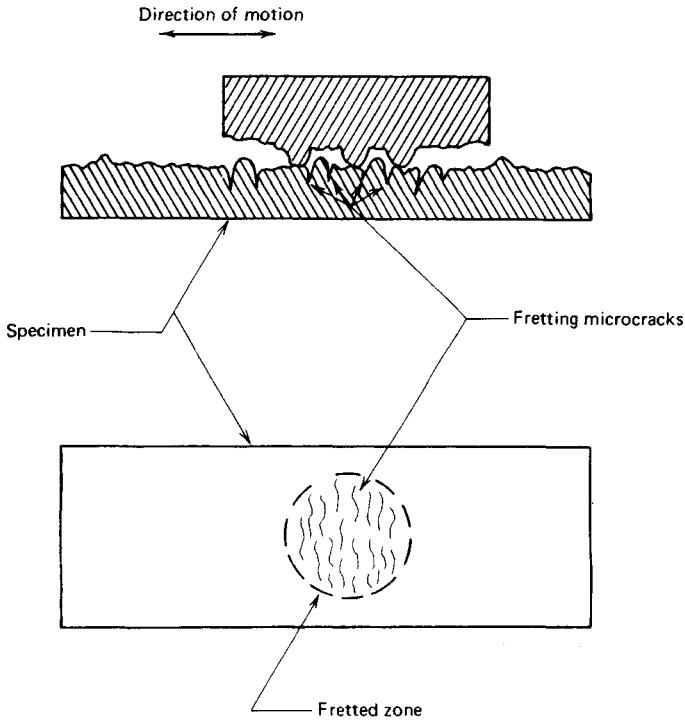


**Fig. 18.71** Idealized schematic illustration of the stress concentrations produced by the asperity-contact microcrack initiation mechanism.

In the delamination theory of fretting<sup>112</sup> it is hypothesized that the combination of normal and tangential tractive forces transmitted through the asperity-contact sites at the fretting interface produce a complex multiaxial state of stress, accompanied by a cycling deformation field, which produces subsurface peak shearing stress and subsurface crack nucleation sites. With further cycling, the cracks propagate approximately parallel to the surface, as in the case of the surface fatigue phenomenon, finally propagating to the surface to produce a thin wear sheet, which "delaminates" to become a particle of debris.

Supporting evidence has been generated to indicate that under various circumstances each of the four mechanisms is active and significant in producing fretting damage.

The influence of the state of stress in the member during the fretting is shown for several different cases in Fig. 18.73, including static tensile and compressive mean stresses during fretting. An interesting observation in Fig. 18.73 is that fretting under conditions of compressive mean stress, either static or cyclic, produces a drastic reduction in fatigue properties. This, at first, does not seem to be in keeping with the concept that compressive stresses are beneficial in fatigue loading. However, it was deduced<sup>121</sup> that the compressive stresses during fretting shown in Fig. 18.73 actually resulted in local residual tensile stresses in the fretted region. Likewise, the tensile stresses during fretting shown in Fig. 18.73 actually resulted in local residual compressive stresses in the fretted region. The conclusion, therefore, is that local compressive stresses are beneficial in minimizing fretting fatigue damage.

Further evidence of the beneficial effects of compressive residual stresses in minimizing fretting fatigue damage is illustrated in Fig. 18.74, where the results of a series of Prot (fatigue limit) tests are reported for steel and titanium specimens subjected to various combinations of shot peening and fretting or cold rolling and fretting. It is clear from these results that the residual compressive stresses produced by shot peening and cold rolling are effective in minimizing the fretting damage. The reduction in scatter of the fretted fatigue properties for titanium is especially important to a designer because design stress is closely related to the lower limit of the scatter band.

Recent efforts to apply the tools of fracture mechanics to the problem of life prediction under fretting fatigue conditions have produced encouraging preliminary results that may ultimately provide designers with a viable quantitative approach.<sup>122</sup> These studies emphasize that the principal effect of fretting in the fatigue failure process is to accelerate crack initiation and the early stages of crack growth, and they suggest that when cracks have reached a sufficient length, the fretting no longer

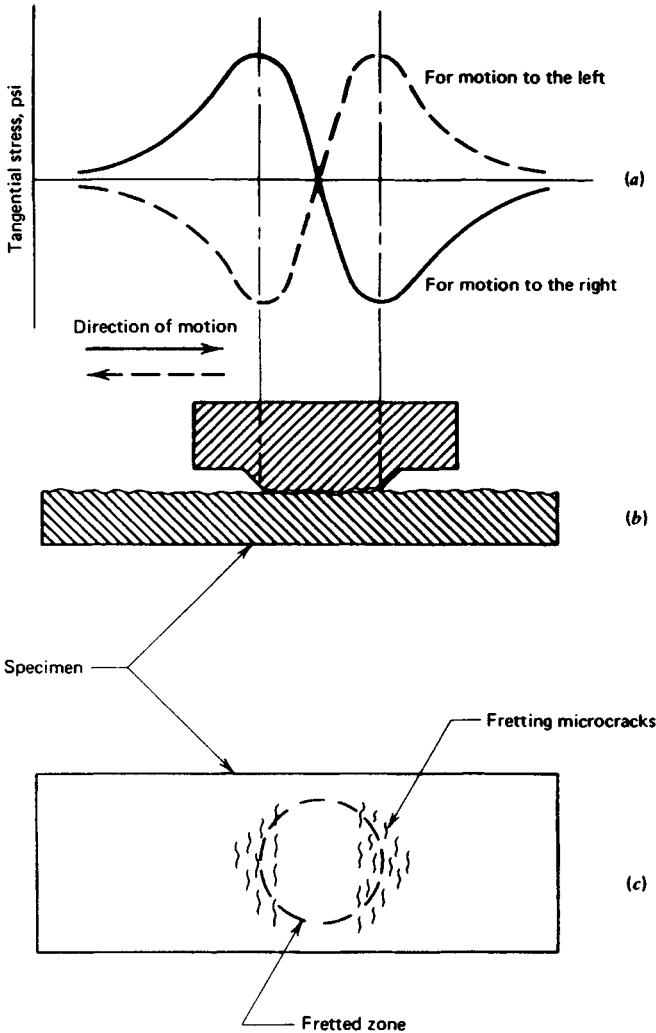


**Fig. 18.72** Idealized schematic illustration of the tangential stress components and microcracks produced by the friction-generated microcrack initiation mechanism.

has a significant influence on crack propagation. At this point the fracture mechanics description of crack propagation described in Section 18.5.8 becomes valid.

In the final analysis, it is necessary to evaluate the seriousness of fretting fatigue damage in any specific design by running simulated service tests on specimens or components. Within the current state-of-the-art knowledge in the area of fretting fatigue, there is no other safe course of action open to the designer.

Fretting wear is a change in dimensions through wear directly attributable to the fretting process between two mating surfaces. It is thought that the abrasive pit-digging mechanism, the asperity-contact microcrack initiation mechanism, and the wear-sheet delamination mechanism may all be important in most fretting wear failures. As in the case of fretting fatigue, there has been no good model developed to describe the fretting wear phenomenon in a way useful for design. An expression for weight loss due to fretting has been proposed<sup>102</sup> as

$$W_{\text{total}} = (k_0 L^{1/2} - k_1 L) \frac{C}{F} + k_2 SLC \tag{18.86}$$

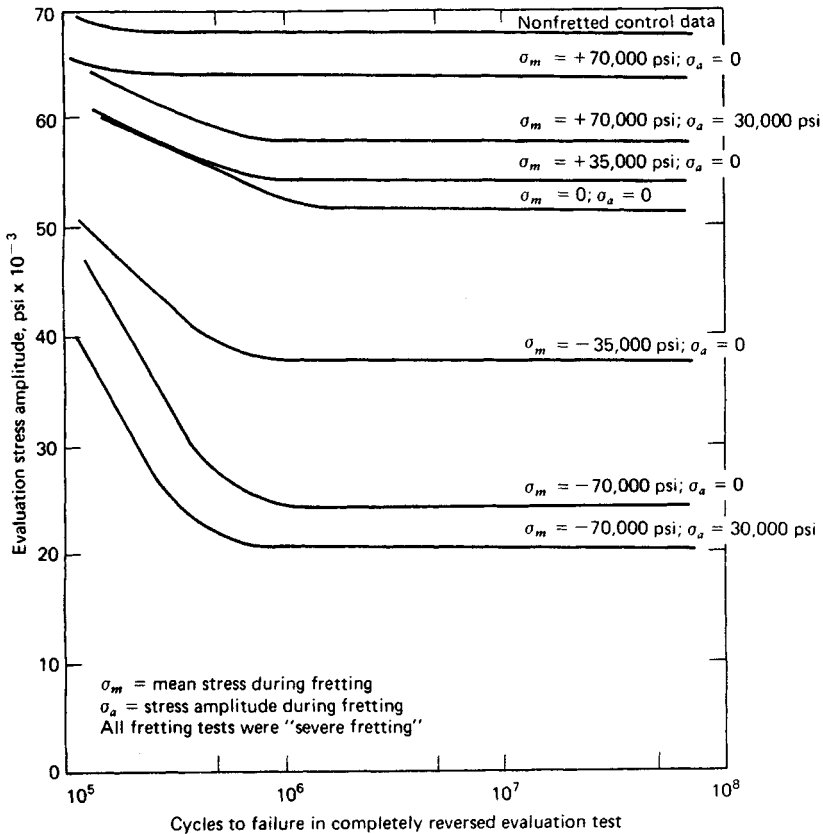


Fig. 18.73 Residual fatigue properties subsequent to fretting under various states of stress.

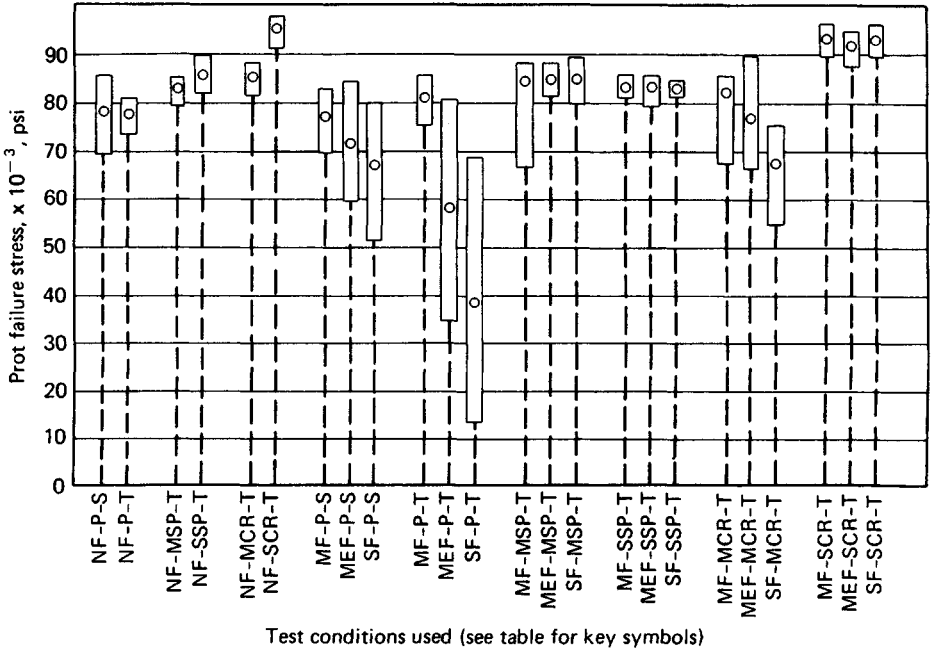
where  $W_{total}$  = total specimen weight loss  
 $L$  = normal contact load  
 $C$  = number of fretting cycles  
 $F$  = frequency of fretting  
 $S$  = peak-to-peak slip between fretting surfaces  
 $k_0, k_1, k_2$  = constants to be empirically determined

This equation has been shown to give relatively good agreement with experimental data over a range of fretting conditions using mild steel specimens.<sup>102</sup> However, weight loss is not of direct use to a designer. Wear depth is of more interest. Prediction of wear depth in an actual design application must in general be based on simulated service testing.

Some investigators have suggested that estimates of fretting wear depth may be based on the classical adhesive or abrasive wear equations, in which wear depth is proportional to load and total distance slid, where the total distance slid is calculated by multiplying relative motion per cycle times number of cycles. Although there are some supporting data for such a procedure,<sup>123</sup> more investigation is required before it could be recommended as an acceptable approach for general application.

If fretting wear at a support interface, such as between tubes and support plates of a steam generator or heat exchanger or between fuel pins and support grids of a reactor core, produces loss of fit at a support site, impact fretting may occur. Impact fretting is fretting action induced by the small lateral relative displacements between two surfaces when they impact together, where the small displacements are caused by Poisson strains or small tangential "glancing" velocity components. Impact fretting has only recently been addressed in the literature,<sup>124</sup> but it should be noted that under certain circumstances impact fretting may be a potential failure mode of great importance.

Fretting corrosion may be defined as any corrosive surface involvement resulting as a direct result of fretting action. The consequences of fretting corrosion are generally much less severe than for either fretting wear or fretting fatigue. Note that the term *fretting corrosion* is not being used here



Test Condition Used	Code Designation	Sample Size	Mean Prot Failure Stress, psi	Unbiased Standard Deviation, psi
Nonfretted, polished, SAE 4340 steel	NF-P-S	15	78,200	5,456
Nonfretted, polished, Ti-140-A titanium	NF-P-T	15	77,800	2,454
Nonfretted, mildly shot-peened, Ti-140-A titanium	NF-MSP-T	15	83,100	1,637
Nonfretted, severely shot-peened, Ti-140-A titanium	NF-SSP-T	15	85,700	2,398
Nonfretted, mildly cold-rolled, Ti-140-A titanium	NF-MCR-T	15	85,430	1,924
Nonfretted, severely cold-rolled, Ti-140-A titanium	NF-SCR-T	15	95,400	2,120
Mildly fretted, polished, SAE 4340 steel	MF-P-S	15	77,280	4,155
Medium fretted, polished, SAE 4340 steel	MeF-P-S	15	71,850	5,492
Severely fretted, polished, SAE 4340 steel	SF-P-S	15	67,700	6,532
Mildly fretted, polished, Ti-140-A titanium	MF-P-T	15	81,050	3,733
Medium fretted, polished, Ti-140-A titanium	MeF-P-T	15	58,140	15,715
Severely fretted, polished, Ti-140-A titanium	SF-P-T	15	38,660	19,342
Mildly fretted, mildly shot-peened, Ti-140-A titanium	MF-MSP-T	15	84,520	5,239
Medium fretted, mildly shot-peened, Ti-140-A titanium	MeF-MSP-T	15	84,930	2,446
Severely fretted, mildly shot-peened, Ti-140-A titanium	SF-MSP-T	15	84,870	2,647
Mildly fretted, severely shot-peened, Ti-140-A titanium	MF-SSP-T	15	83,600	1,474
Medium fretted, severely shot-peened, Ti-140-A titanium	MeF-SSP-T	15	83,240	1,332
Severely fretted, severely shot-peened, Ti-140-A titanium	SF-SSP-T	15	83,110	1,280
Mildly fretted, mildly cold-rolled, Ti-140-A titanium	MF-MCR-T	15	82,050	4,313
Medium fretted, mildly cold-rolled, Ti-140-A titanium	MeF-MCR-T	15	76,930	8,305
Severely fretted, mildly cold-rolled, Ti-140-A titanium	SF-MCR-T	15	67,960	5,682
Mildly fretted, severely cold-rolled, Ti-140-A titanium	MF-SCR-T	15	93,690	1,858
Medium fretted, severely cold-rolled, Ti-140-A titanium	MeF-SCR-T	15	91,950	2,098
Severely fretted, severely cold-rolled, Ti-140-A titanium	SF-SCR-T	15	93,150	1,365

Fig. 18.74 Fatigue properties of fretted steel and titanium specimens with various degrees of shot peening and cold rolling. (See Ref. 106.)

as a synonym for fretting, as in much of the early literature on this topic. Perhaps the most important single parameter in minimizing fretting corrosion is proper selection of the material pair for the application. Table 18.5 lists a variety of material pairs grouped according to their resistance to fretting corrosion.<sup>125</sup> Cross comparisons from one investigator's results to another's must be made with care because testing conditions varied widely. The minimization or prevention of fretting damage must be carefully considered as a separate problem in each individual design application because a palliative in one application may significantly accelerate fretting damage in a different application. For example, in a joint that is designed to have no relative motion, it is sometimes possible to reduce or prevent fretting by increasing the normal pressure until all relative motion is arrested. However, if the increase in normal pressure does not completely arrest the relative motion, the result may be significantly increasing fretting damage instead of preventing it.

Nevertheless, there are several basic principles that are generally effective in minimizing or preventing fretting. These include:

1. Complete separation of the contacting surfaces.
2. Elimination of all relative motion between the contacting surfaces.
3. If relative motion cannot be eliminated, it is sometimes effective to superpose a large unidirectional relative motion that allows effective lubrication. For example, the practice of driving the inner or outer race of an oscillatory pivot bearing may be effective in eliminating fretting.
4. Providing compressive residual stresses at the fretting surface; this may be accomplished by shot peening, cold rolling, or interference fit techniques.
5. Judicious selection of material pairs.
6. Use of interposed low-shear-modulus shim material or plating, such as lead, rubber, or silver.
7. Use of surface treatments or coatings as solid lubricants.
8. Use of surface grooving or roughening to provide debris escape routes and differential strain matching through elastic action.

Of all these techniques, only the first two are completely effective in preventing fretting. The remaining concepts, however, may often be used to minimize fretting damage and yield an acceptable design.

### 18.8.2 Wear Phenomena

The complexity of the wear process may be better appreciated by recognizing that many variables are involved, including the hardness, toughness, ductility, modulus of elasticity, yield strength, fatigue properties, and structure and composition of the mating surfaces, as well as geometry, contact pressure, temperature, state of stress, stress distribution, coefficient of friction, sliding distance, relative velocity, surface finish, lubricants, contaminants, and ambient atmosphere at the wearing interface. Clearance versus contact-time history of the wearing surfaces may also be an important factor in some cases. Although the wear processes are complex, progress has been made in recent years toward development of quantitative empirical relationships for the various subcategories of wear under specified operating conditions. Adhesive wear is often characterized as the most basic or fundamental subcategory of wear since it occurs to some degree whenever two solid surfaces are in rubbing contact and remains active even when all other modes of wear have been eliminated. The phenomenon of adhesive wear may be best understood by recalling that all real surfaces, no matter how carefully prepared and polished, exhibit a general waviness upon which is superposed a distribution of local protuberances or asperities. As two surfaces are brought into contact, therefore, only a relatively few asperities actually touch, and the *real* area of contact is only a small fraction of the *apparent* contact area. (See Chap. 1 of Ref. 126 and Chap. 2 of Ref. 127.) Thus, even under very small applied loads the local pressures at the contact sites become high enough to exceed the yield strength of one or both surfaces, and local plastic flow ensues. If the contacting surfaces are clean and uncorroded, the very intimate contact generated by this local plastic flow brings the atoms of the two contacting surfaces close enough together to call into play strong adhesive forces. This process is sometimes called *cold welding*. Then if the surfaces are subjected to relative sliding motion, the cold-welded junctions must be broken. Whether they break at the original interface or elsewhere within the asperity depends on surface conditions, temperature distribution, strain-hardening characteristics, local geometry, and stress distribution. If the junction is broken away from the original interface, a particle of one surface is transferred to the other surface, marking one event in the adhesive wear process. Later sliding interactions may dislodge the transferred particles as loose wear particles, or they may remain attached. If this adhesive wear process becomes severe and large-scale metal transfer takes place, the phenomenon is called *galling*. If the galling becomes so severe that two surfaces adhere over a large region so that the actuating forces can no longer produce relative motion between them, the phenomenon is called *seizure*. If properly controlled, however, the adhesive wear rate may be

**Table 18.5 Fretting Corrosion Resistance of Various Material Pairs<sup>125</sup>**

<i>Material Pairs Having Good Fretting Corrosion Resistance</i>			
Sakmann and Rightmire	Lead	on	Steel
	Silver plate	on	Steel
	Silver plate	on	Silver plate
	'Parco-lubrized' steel	on	Steel
Gray and Jenny	Grit blasted steel plus lead plate	on	Steel (very good)
	1/16 in. nylon insert	on	Steel (very good)
	Zinc and iron phosphated (Bonderizing) steel	on	Steel (good with thick coat)
McDowell	Laminated plastic	on	Gold plate
	Hard tool steel	on	Tool steel
	Cold-rolled steel	on	Cold-rolled steel
	Cast iron	on	Cast iron with phosphate coating
	Cast iron	on	Cast iron with rubber cement
	Cast iron	on	Cast iron with tungsten sulphide coating
	Cast iron	on	Cast iron with rubber insert
	Cast iron	on	Cast iron with Molykote lubricant
	Cast iron	on	Stainless steel with Molykote lubricant
<i>Material Pairs Having Intermediate Fretting Corrosion Resistance</i>			
Sakmann and Rightmire	Cadmium	on	Steel
	Zinc	on	Steel
	Copper alloy	on	Steel
	Zinc	on	Aluminum
	Copper plate	on	Aluminum
	Nickel plate	on	Aluminum
	Silver plate	on	Aluminum
	Iron plate	on	Aluminum
Gray and Jenny	Sulphide coated bronze	on	Steel
	Cast bronze	on	"Parco-lubrized" steel
	Magnesium	on	"Parco-lubrized" steel
	Grit-blasted steel	on	Steel
McDowell	Cast iron	on	Cast iron (rough or smooth surface)
	Copper	on	Cast iron
	Brass	on	Cast iron
	Zinc	on	Cast iron
	Cast iron	on	Silver plate
	Cast iron	on	Copper plate
	Magnesium	on	Copper plate
	Zirconium	on	Zirconium
Sakmann and Rightmire	Steel	on	Steel
	Nickel	on	Steel
	Aluminum	on	Steel
	Al-Si alloy	on	Steel
	Antimony plate	on	Steel
	Tin	on	Steel
	Aluminium	on	Aluminum
	Zinc plate	on	Aluminum
Gray and Jenny	Grit blast plus silver plate	on	Steel*
	Steel	on	Steel
	Grit blast plus copper plate	on	Steel
	Grit blast plus tin plate	on	Steel
	Grit blast and aluminium foil	on	Steel
	Be-Cu insert	on	Steel
	Magnesium	on	Steel
	Nitrided steel	on	Chromium plated steel†

**Table 18.5 (Continued)**

<i>Material Pairs Having Poor Fretting Corrosion Resistance</i>		
McDowell	Aluminium	on Cast iron
	Aluminium	on Stainless steel
	Magnesium	on Cast iron
	Cast iron	on Chromium plate
	Laminated plastic	on Cast iron
	Bakelite	on Cast iron
	Hard tool steel	on Stainless steel
	Chromium plate	on Chromium plate
	Cast iron	on Tin plate
	Gold plate	on Gold plate

\*Possibly effective with light loads and thick (0.005 inch) silver plate.

†Some improvement by heating chromium plated steel to 538°C for 1 hour.

low and self-limiting, often being exploited in the “wearing-in” process to improve mating surfaces such as bearings or cylinders so that full film lubrication may be effectively used.

One quantitative estimate of the amount of adhesive wear is given as follows (see Ref. 113 and Chaps. 2 and 6 of Ref. 128):

$$d_{\text{adh}} = \frac{V_{\text{adh}}}{A_a} = \left( \frac{k}{9\sigma_{yp}} \right) \left( \frac{W}{A_a} \right) L_s \quad (18.87)$$

or

$$d_{\text{adh}} = k_{\text{adh}} p_m L_s \quad (18.88)$$

where  $d_{\text{adh}}$  is the average wear depth,  $A_a$  is the apparent contact area,  $L_s$  is the total sliding distance,  $V_{\text{adh}}$  is the wear volume,  $W$  is the applied load,  $p_m = W/A_a$  is the mean nominal contact pressure between bearing surfaces, and  $k_{\text{adh}} = k/9\sigma_{yp}$  is a wear coefficient that depends on the probability of formation of a transferred fragment and the yield strength (or hardness) of the softer material. Typical values of the wear constant  $k$  for several material pairs are shown in Table 18.6, and the influence of lubrication on the wear constant  $k$  is indicated in Table 18.7.

Noting from (18.88) that

$$k_{\text{adh}} = \frac{d_{\text{adh}}}{p_m L_s} \quad (18.89)$$

it may be observed that if the ratio  $d_{\text{adh}}/p_m L_s$  is experimentally found to be constant, (18.88) should be valid. Experimental evidence has been accumulated (see pp. 124–125 of Ref. 113) to confirm that for a given material pair this ratio is constant up to mean nominal contact pressures approximately equal to the uniaxial yield strength. Above this level the adhesive wear coefficient increases rapidly, with attendant severe galling and seizure.

**Table 18.6 Archard Adhesive Wear Constant  $k$  for Various Unlubricated Material Pairs in Sliding Contact<sup>a</sup>**

Material Pair	Wear Constant $k$
Zinc on zinc	$160 \times 10^{-3}$
Low-carbon steel on low-carbon steel	$45 \times 10^{-3}$
Copper on copper	$32 \times 10^{-3}$
Stainless steel on stainless steel	$21 \times 10^{-3}$
Copper (on low-carbon steel)	$1.5 \times 10^{-3}$
Low-carbon steel (on copper)	$0.5 \times 10^{-3}$
Bakelite on bakelite	$0.02 \times 10^{-3}$

<sup>a</sup>From Chap. 6 of Ref. 128, with permission of John Wiley & Sons.

**Table 18.7 Order of Magnitude Values for Adhesive Wear Constant  $k$  Under Various Conditions of Lubrication<sup>a</sup>**

Lubrication Condition	Metal (on Metal)		Nonmetal (on Metal)
	Like	Unlike	
Unlubricated	$5 \times 10^{-3}$	$2 \times 10^{-4}$	$5 \times 10^{-6}$
Poorly lubricated	$2 \times 10^{-4}$	$2 \times 10^{-4}$	$5 \times 10^{-6}$
Average lubrication	$2 \times 10^{-5}$	$2 \times 10^{-5}$	$5 \times 10^{-6}$
Excellent lubrication	$2 \times 10^{-6}$ to $10^{-7}$	$2 \times 10^{-6}$ to $10^{-7}$	$2 \times 10^{-6}$

<sup>a</sup>From Chap. 6 of Ref. 128, with permission of John Wiley & Sons.

In the selection of metal combinations to provide resistance to adhesive wear, it has been found that the sliding pair should be composed of mutually insoluble metals and that at least one of the metals should be from the B subgroup of the periodic table. (See p. 31 of Ref. 129.) The reasons for these observations are that the number of cold-weld junctions formed is a function of the mutual solubility, and the strength of the junction bonds is a function of the bonding characteristics of the metals involved. The metals in the B subgroup of the periodic table are characterized by weak, brittle covalent bonds. These criteria have been verified experimentally, as shown in Table 18.8, where 114 of 123 pairs tested substantiated the criteria.

In the case of abrasive wear, the wear particles are removed from the surface by the plowing and gouging action of the asperities of a harder mating surface or by hard particles trapped between the rubbing surfaces. This type of wear is manifested by a system of surface grooves and scratches, often called *scoring*. The abrasive wear condition in which the hard asperities of one surface wear away the mating surface is commonly called *two-body wear*, and the condition in which hard abrasive particles between the two surfaces cause the wear is called *three-body wear*.

An average abrasive wear depth  $d_{abr}$  may then be estimated as

$$d_{abr} = \frac{V_{abr}}{A_a} = \frac{(\tan \theta)_m}{3\pi\sigma_{yp}} \left( \frac{W}{A_a} \right) L_s \quad (18.90)$$

or

$$d_{abr} = k_{abr} p_m L_s \quad (18.91)$$

where  $W$  is total applied load,  $(\tan \theta)_m$  is a weighted mean value for all asperities,  $L_s$  is a total distance of sliding,  $\sigma_{yp}$  is the uniaxial yield point strength for the softer material,  $V_{abr}$  is abrasive wear volume,  $p_m = W/A_a$  is mean nominal contact pressure between bearing surfaces, and  $k_{abr} = (\tan \theta)_m / 3\pi\sigma_{yp}$  is an abrasive wear coefficient that depends on the roughness characteristics of the surface and the yield strength (or hardness) of the softer material.

Comparing (18.90) for abrasive wear volume with (18.87) for adhesive wear volume, we note that they are formally the same except the constant  $k/3$  in the adhesive wear equation is replaced by  $(\tan \theta)_m / \pi$  in the abrasive wear equation. Typical values of the wear constant  $3(\tan \theta)_m / \pi$  for several materials are shown in Table 18.9. As indicated in Table 18.9, experimental evidence shows that  $k_{abr}$  for three-body wear is typically about an order of magnitude smaller than for the two-body case, probably because the trapped particles tend to roll much of the time and cut only a small part of the time.

In selecting materials for abrasive wear resistance, it has been established that both hardness and modulus of elasticity are key properties. Increasing wear resistance is associated with higher hardness and lower modulus of elasticity since both the amount of elastic deformation and the amount of elastic energy that can be stored at the surface are increased by higher hardness and lower modulus of elasticity.

Table 18.10 tabulates several materials in order of descending values of (hardness)/(modulus of elasticity). Well-controlled experimental data are not yet available, but general experience would provide an ordering of materials for decreasing wear resistance compatible with the array of Table 18.10. When the conditions for adhesive or abrasive wear exist together with conditions that lead to corrosion, the two processes persist together and often interact synergistically. If the corrosion product is hard and abrasive, dislodged corrosion particles trapped between contacting surfaces will accelerate the abrasive wear process. In turn, the wear process may remove the "protective" surface layer of corrosion product to bare new metal to the corrosive atmosphere, thereby accelerating the corrosion process. Thus, the corrosion wear process may be self-accelerating and may lead to high rates of wear.

Table 18.8 Adhesive Wear Behavior of Various Pairs<sup>a</sup>

Description of Metal Pair	Material Combination				Remarks
	Al Disk	Steel Disk	Cu Disk	Ag Disk	
Soluble pairs with poor adhesive wear resistance	Be	Be	Be	Be	These pairs substantiate the criteria of solubility and B subgroup metals
	Mg	—	Mg	Mg	
	Al	Al	Al	—	
	Si	Si	Si	Si	
	Ca	—	Ca	—	
	Ti	Ti	Ti	—	
	Cr	Cr	—	—	
	—	Mn	—	—	
	Fe	Fe	—	—	
	Co	Co	Co	—	
	Ni	Ni	Ni	—	
	Cu	—	Cu	—	
	—	Zn	Zn	—	
	Zr	Zr	Zr	Zr	
	Nb	Nb	Nb	—	
	Mo	Mo	Mo	—	
	Rh	Rh	Rh	—	
	—	Pd	—	—	
	Ag	—	Ag	—	
	—	—	Cd	Cd	
	—	—	In	In	
	Sn	—	Sn	—	
	Ce	Ce	Ce	—	
	Ta	Ta	Ta	—	
	W	W	W	—	
	—	Ir	—	—	
Pt	Pt	Pt	—		
Au	Au	Au	Au		
Th	Th	Th	Th		
U	U	U	U		
Soluble pairs with fair or good adhesive wear resistance. (F) = Fair	—	Cu(F)	—	These pairs do not substantiate the stated criteria	
	Zn(F)	—	—		
	—	—	Sb(F)		
Insoluble pairs, neither from the B subgroup, with poor adhesive wear resistance	—	Li	—	These pairs substantiate the stated criteria	
	—	Mg	—		
	—	Ca	—		
	—	Ba	—		
Insoluble pairs, one from the B subgroup, with fair or good adhesive wear resistance. (F) = Fair	—	C(F)	—	These pairs substantiate the stated criteria	
	—	—	—		
	—	—	Cr(F)		
	—	—	—		
	—	—	—		
	—	—	—		
	—	—	Ge(F)		
	—	Se(F)	Se(F)		
	—	—	—		
	—	—	Nb(F)		
	—	Ag	—		
	Cd	Cd	—		
	In	In	—		
	—	Sn(F)	—		
	—	Sb(F)	Sb		
	Te(F)	Te(F)	Te(F)		
Tl	Tl	Tl			
Pb(F)	Pb	Pb			
Bi(F)	Bi	Bi(F)			
Insoluble pairs, one from the B subgroup, with poor adhesive wear resistance	C	—	C	These pairs do not substantiate the stated criteria	
	—	—	—		
	Se	—	—		
	—	—	—		
—	—	—	Mo		

<sup>a</sup>See pp. 34–35 of Ref. 129.

**Table 18.9 Abrasive Wear Constant  $3(\tan \theta)_m / \pi$  for Various Materials in Sliding Contact as Reported by Different Investigators<sup>a</sup>**

Materials	Wear Type	Particle Size, $\mu$	$3(\tan \theta)_m / \pi$
Many	Two-body	—	$180 \times 10^{-3}$
Many	Two-body	110	$150 \times 10^{-3}$
Many	Two-body	40–150	$120 \times 10^{-3}$
Steel	Two-body	260	$80 \times 10^{-3}$
Many	Two-body	80	$24 \times 10^{-3}$
Brass	Two-body	70	$16 \times 10^{-3}$
Steel	Three-body	150	$6 \times 10^{-3}$
Steel	Three-body	80	$4.5 \times 15^{-3}$
Many	Three-body	40	$2 \times 10^{-3}$

<sup>a</sup>See p. 169 of Ref. 128. Reprinted with permission from John Wiley & Sons.

On the other hand, some corrosion products, for example, metallic phosphates, sulfides, and chlorides, form as soft lubricative films that actually improve the wear rate markedly, especially if adhesive wear is the dominant phenomenon.

Three major wear control methods have been defined, as follows (see p. 36 of Ref. 129): *principle of protective layers*, including protection by lubricant, surface film, paint, plating, phosphate, chemical, flame-sprayed, or other types of interfacial layers: *principle of conversion*, in which wear is converted from destructive to permissible levels through better choice of metal pairs, hardness, surface finish, or contact pressure; and *principle of diversion*, in which the wear is diverted to an economical replaceable wear element that is periodically discarded and replaced as “wear out” occurs. When two surfaces operate in rolling contact, the wear phenomenon is quite different from the wear of sliding surfaces just described, although the “delamination” theory<sup>130</sup> is very similar to the mechanism of wear between rolling surfaces in contact as described here. Rolling surfaces in contact result

**Table 18.10 Values of (Hardness/Modulus of Elasticity) for Various Materials<sup>113</sup> †**

Material	Condition	BHN* / ( $E \times 10^{-6}$ ) (in mixed units)
Alundum (Al <sub>2</sub> O <sub>3</sub> )	Bonded	143
Chrome plate	Bright	83
Gray iron	Hard	33
Tungsten carbide	9% Co	22
Steel	Hard	21
Titanium	Hard	17
Aluminum alloy	Hard	11
Gray iron	As cast	10
Structural steel	Soft	5
Malleable iron	Soft	5
Wrought iron	Soft	3.5
Chromium metal	As cast	3.5
Copper	Soft	2.5
Silver	Pure	2.3
Aluminum	Pure	2.0
Lead	Pure	2.0
Tin	Pure	0.7

†Reprinted from copyrighted work with permission; courtesy of Elsevier Publishing Company.

\*Brinell hardness number.

in Hertz contact stresses that produce maximum values of shear stress slightly below the surface. (See, for example, p. 389 of Ref. 131.) As the rolling contact zone moves past a given location on the surface, the subsurface peak shear stress cycles from zero to a maximum value and back to zero, thus producing a cyclic stress field. Such conditions may lead to fatigue failure by the initiation of a subsurface crack that propagates under repeated cyclic loading and that may ultimately propagate to the surface to spall out a macroscopic surface particle to form a wear pit. This action, called *surface fatigue wear*, is a common failure mode in antifriction bearings, gears, and cams, and all machine parts that involve rolling surfaces in contact. Deformation wear arises as a result of repeated plastic deformations at the wearing surfaces; this wear may induce a matrix of cracks that grow and coalesce to form wear particles or may produce cumulative permanent plastic deformations that finally grow into an unacceptable surface indentation or wear scar. Deformation wear is generally caused by conditions that lead to impact loading between the two wearing surfaces. Although some progress has been made in deformation wear analysis, the techniques are highly specialized. Fretting wear, which has received renewed attention in the recent literature (see p. 55 of Ref. 132 and p. 75 of Ref. 128), has already been discussed. Impact wear is a term reserved for impact-induced repeated elastic deformations at the wearing surfaces that produce a matrix of cracks that grow in accordance with surface fatigue phenomena. Under some circumstances impact wear may be generated by purely normal impacts, and under other circumstances the impact may contain elements of rolling and/or sliding as well. The severity of the impact is generally measured or expressed in terms of the kinetic energy of the striking mass. The geometry of the impacting surfaces and the material properties of the two contacting surfaces play a major role in the determination of severity of impact wear damage. The objective of a designer faced with impact wear as a potential failure mode is to predict the size of the wear scar, or its depth, as a function of the number of repetitive load cycles.

An *empirical* approach to the prediction of sliding wear has been developed,<sup>133</sup> and the pertinent empirical constants have been evaluated for a wide variety of materials and lubricant combinations for various operating conditions. This empirical development permits the designer to specify a design configuration to ensure "zero wear" during the specified design lifetime. *Zero wear* is defined to be wear of such small magnitude that the surface finish is not significantly altered by the wear process. That is, the wear depth for zero wear is of the order of one-half the peak-to-peak surface finish dimension.

If a *pass* is defined to be a distance of sliding  $W$  equal to the dimension of the contact area in the direction of sliding,  $N$  is the number of passes,  $\tau_{\max}$  is the maximum shearing stress in the vicinity of the surface,  $\tau_{yp}$  is the shear yield point of the specified material, and  $\gamma_r$  is a constant for the particular combination of materials and lubricant, then the empirical model asserts that there will be "zero wear" for  $N$  passes if

$$\tau_{\max} \leq \left[ \frac{2 \times 10^3}{N} \right]^{1/9} \gamma_r \tau_{yp} \quad (18.92)$$

or, to interpret it differently, the number of passes that can be accommodated without exceeding the zero wear level is given by

$$N = 2 \times 10^3 \left[ \frac{\gamma_r \tau_{yp}}{\tau_{\max}} \right]^9 \quad (18.93)$$

It may be noted that the constant  $\gamma_r$  is referred to 2000 passes and must be experimentally determined. For quasihydrodynamic lubrication,  $\gamma_r$  ranges between 0.54 and 1. For dry or boundary lubrication,  $\gamma_r$  is 0.54 for materials with low susceptibility to adhesive wear and 0.20 for materials with high susceptibility to adhesive wear.

Calculation of the maximum shear stress  $\tau_{\max}$  in the vicinity of the contacting surface must include both the normal force and the friction force. Thus, for conforming geometries, such as a flat surface on a flat surface or a shaft in a journal bearing, a critical point at the contacting interface may be analyzed by the maximum shear stress theory to determine  $\tau_{\max}$ .

The number of passes will usually require expression as a function of the number of cycles, strokes, oscillations, or hours of operation in the design lifetime.

Utilizing these definitions and a proper stress analysis at the wear interface allows one to design for "zero wear" through use of Eqs. (18.92) or (18.93).

## 18.9 CORROSION AND STRESS CORROSION

Corrosion may be defined as the undesired deterioration of a material through chemical or electrochemical interaction with the environment, or destruction of materials by means other than purely mechanical action. Failure by corrosion occurs when the corrosive action renders the corroded device incapable of performing its design function. Corrosion often interacts synergistically with another failure mode, such as wear or fatigue, to produce the even more serious combined failure modes, such as corrosion wear or corrosion fatigue. Failure by corrosion and protection against failure by

corrosion has been estimated to cost in excess of 8 billion dollars annually in the United States alone. (See p. 1 of Ref. 134.)

The complexity of the corrosion process may be better appreciated by recognizing that many variables are involved, including environmental, electrochemical, and metallurgical aspects. For example, anodic reactions and rate of oxidation; cathodic reactions and rate of reduction; corrosion inhibition, polarization, or retardation; passivity phenomena; effect of oxidizers; effect of velocity; temperature; corrosive concentration; galvanic coupling; and metallurgical structure all influence the type and rate of the corrosion process.

Corrosion processes have been categorized in many different ways. One convenient classification divides corrosion phenomena into the following types (see p. 28 of Ref. 134 and p. 85 of Ref. 135): direct chemical attack, galvanic corrosion, crevice corrosion, pitting corrosion, intergranular corrosion, selective leaching, erosion corrosion, cavitation corrosion, hydrogen damage, biological corrosion, and stress corrosion cracking. Depending on the types of environment, loading, and mechanical function of the machine parts involved, any of the types of corrosion may combine their influence with other failure modes to produce premature failures. Of particular concern are interactions that lead to failure by corrosion wear, corrosion fatigue, fretting fatigue, and corrosion-induced brittle fracture.

### 18.9.1 Types of Corrosion

Direct chemical attack is probably the most common type of corrosion. Under this type of corrosive attack the surface of the machine part exposed to the corrosive media is attacked more or less uniformly over its entire surface, resulting in a progressive deterioration and dimensional reduction of sound load-carrying net cross section. The rate of corrosion due to direct attack can usually be estimated from relatively simple laboratory tests in which small specimens of the selected material are exposed to a well-simulated actual environment, with frequent weight change and dimensional measurements carefully taken. The corrosion rate is usually expressed in mils per year (mpy) and may be calculated as (see p. 133 of Ref. 134)

$$R = \frac{534W}{\gamma A t} \quad (18.94)$$

where  $R$  is rate of corrosion penetration in mils (1 mil = 0.001 in.) per year (mpy),  $W$  is weight loss in milligrams,  $A$  is exposed area of the specimen in square inches,  $\gamma$  is density of the specimen in grams per cubic centimeter, and  $t$  is exposure time in hours. Use of this corrosion rate expression in predicting corrosion penetration in actual service is usually successful if the environment has been properly simulated in the laboratory. Corrosion rate data for many different combinations of materials and environments are available in the literature.<sup>136-138</sup> Figure 18.75 illustrates one presentation of such data.

Direct chemical attack may be reduced in severity or prevented by any one or a combination of several means, including selecting proper materials to suit the environment; using plating, flame spraying, cladding, hot dipping, vapor deposition, conversion coatings, and organic coatings or paint to protect the base material; changing the environment by using lower temperature or lower velocity, removing oxygen, changing corrosive concentration, or adding corrosion inhibitors; using cathodic protection in which electrons are supplied to the metal surface to be protected either by galvanic coupling to a sacrificial anode or by an external power supply; or adopting other suitable design modifications.

Galvanic corrosion is an accelerated electrochemical corrosion that occurs when two dissimilar metals in electrical contact are made part of a circuit completed by a connecting pool or film of electrolyte or corrosive medium. Under these circumstances, the potential difference between the dissimilar metals produces a current flow through the connecting electrolyte, which leads to corrosion, concentrated primarily in the more anodic or less noble metal of the pair. This type of action is completely analogous to a simple battery cell. Current must flow to produce galvanic corrosion, and, in general, more current flow means more serious corrosion. The relative tendencies of various metals to form galvanic cells, and the probable direction of the galvanic action, are illustrated for several commercial metals and alloys in seawater in Table 18.11. (See p. 32 of Ref. 134 or p. 86 of Ref. 135.)

Ideally, tests in the actual service environment should be conducted; but, if such data are unavailable, the data of Table 18.11 should give a good indication of possible galvanic action. The farther apart the two dissimilar metals are in the galvanic series, the more serious the galvanic corrosion problem may be. Material pairs within any bracketed group exhibit little or no galvanic action. It should be noted, however, that there are sometimes exceptions to the galvanic series of Table 18.11, so wherever possible corrosion tests should be performed with actual materials in the actual service environment.

The accelerated galvanic corrosion is usually most severe near the junction between the two metals, decreasing in severity at locations farther from the junction. The ratio of cathodic area to anodic area exposed to the electrolyte has a significant effect on corrosion rate. It is *desirable* to

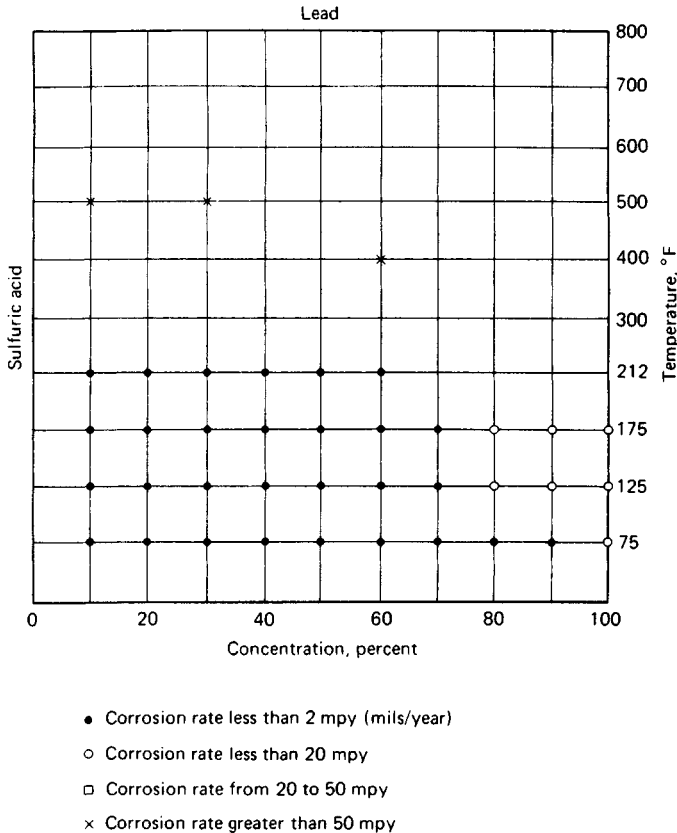


**Fig. 18.75** Nelson's method for summarizing corrosion rate data for lead in sulfuric acid environment as a function of concentration and temperature. (See Ref. 136; reprinted with permission of McGraw-Hill Book Company.)

have a *small ratio* of cathode area to anode area. For this reason, if only *one* of two dissimilar metals in electrical contact is to be coated for corrosion protection, the *more* noble or more corrosion-resistant metal should be coated. Although this at first may seem the wrong metal to coat, the area effect, which produces anodic corrosion rate of  $10^2$ – $10^3$  times cathodic corrosion rates for equal areas, provides the logic for this assertion.

Galvanic corrosion may be reduced in severity or prevented by one or a combination of several steps, including the selection of material pairs as close together as possible in the galvanic series, preferably in the same bracketed group; electrical insulation of one dissimilar metal from the other as completely as possible; maintaining as small a ratio of cathode area to anode area as possible; proper use and maintenance of coatings; the use of inhibitors to decrease the aggressiveness of the corroding medium; and the use of cathodic protection in which a third metal element anodic to both members of the operating pair is used as a sacrificial anode that may require periodic replacement.

Crevice corrosion is an accelerated corrosion process highly localized within crevices, cracks, and other small-volume regions of stagnant solution in contact with the corroding metal. For example, crevice corrosion may be expected in gasketed joints; clamped interfaces; lap joints; rolled joints; under bolt and rivet heads; and under foreign deposits of dirt, sand, scale, or corrosion product. Until recently, crevice corrosion was thought to result from differences in either oxygen concentration or metal ion concentration in the crevice compared to its surroundings. More recent studies seem to indicate, however, that the local oxidation and reduction reactions result in oxygen depletion in the stagnant crevice region, which leads to an excess positive charge in the crevice due to increased metal ion concentration. This, in turn, leads to a flow of chloride and hydrogen ions into the crevice, both of which accelerate the corrosion rate within the crevice. Such accelerated crevice corrosion is highly localized and often requires a lengthy incubation period of perhaps many months before it gets under way. Once started, the rate of corrosion accelerates to become a serious problem. To be

**Table 18.11 Galvanic Series of Several Commercial Metals and Alloys in Seawater<sup>a</sup>**

↑ Noble or cathodic (protected end)	Platinum
	Gold
	Graphite
	Titanium
	Silver
	[Chlorimet 3 (62 Ni, 18 Cr, 18 Mo)]
	[Hastelloy C (62 Ni, 17 C, 15 Mo)]
	[18-8 Mo stainless steel (passive)]
	[18-8 stainless steel (passive)]
	[Chromium stainless steel 11-30% Cr (passive)]
	[Inconel (passive)(80 Ni, 13 Cr, 7 Fe)]
	[Nickel (passive)]
	Silver solder
	[Monel (70 Ni, 30 Cu)]
	[Cupronickels (60-90 Cu, 40-10 Ni)]
[Bronzes (Cu-Sn)]	
[Copper]	
[Brasses (Cu-Zn)]	
[Chlorimet 2 (66 Ni, 32 Mo, 1 Fe)]	
[Hastelloy B (60 Ni, 30 Mo, 6 Fe, 1 Mn)]	
[Inconel (active)]	
[Nickel (active)]	
Tin	
Lead	
Lead-tin solders	
[18-8 Mo stainless steel (active)]	
[18-8 stainless steel (active)]	
Ni-Resist (high Ni cast iron)	
Chromium stainless steel, 13% Cr (active)	
[Cast iron]	
[Steel or iron]	
Active or anodic (corroded end)	2024 aluminum (4.5 Cu, 1.5 Mg, 0.6 Mn)
	Cadmium
	Commercially pure aluminum (1100)
	Zinc
↓	Magnesium and magnesium alloys

<sup>a</sup>See p. 32 of Ref. 134. Reprinted with permission of McGraw-Hill Book Company.

susceptible to crevice corrosion attack, the stagnant region must be wide enough to allow the liquid to enter but narrow enough to maintain stagnation. This usually implies cracks and crevices of a few thousandths to a few hundredths of an inch in width.

To reduce the severity of crevice corrosion, or prevent it, it is necessary to eliminate the cracks and crevices. This may involve caulking or seal welding existing lap joints; redesign to replace riveted or bolted joints by sound, welded joints; filtering foreign material from the working fluid; inspection and removal of corrosion deposits; or using nonabsorbent gasket materials. Pitting corrosion is a very localized attack that leads to the development of an array of holes or pits that penetrate the metal. The pits, which typically are about as deep as they are across, may be widely scattered or so heavily concentrated that they simply appear as a rough surface. The mechanism of pit growth is virtually identical to that of crevice corrosion described, except that an existing crevice is not required to initiate pitting corrosion. The pit is probably initiated by a momentary attack due to a random variation in fluid concentration or a tiny surface scratch or defect. Some pits may become inactive

because of a stray convective current, whereas others may grow large enough to provide a stagnant region of stable size, which then continues to grow over a long period of time at an accelerating rate. Pits usually grow in the direction of the gravity force field since the dense concentrated solution in a pit is required for it to grow actively. Most pits, therefore, grow downward from horizontal surfaces to ultimately perforate the wall. Fewer pits are formed on vertical walls, and very few pits grow upward from the bottom surface.

Measurement and assessment of pitting corrosion damage is difficult because of its highly local nature. Pit depth varies widely and, as in the case of fatigue damage, a statistical approach must be taken in which the probability of a pit of specified depth may be established in laboratory testing. Unfortunately, a significant size effect influences depth of pitting, and this must be taken into account when predicting service life of a machine part based on laboratory pitting corrosion data.

The control or prevention of pitting corrosion consists primarily of the wise selection of material to resist pitting or, since pitting is usually the result of stagnant conditions, imparting velocity to the fluid. Increasing its velocity may also decrease pitting corrosion attack.

Because of the atomic mismatch at the grain boundaries of polycrystalline metals, the stored strain energy is higher in the grain boundary regions than in the grains themselves. These high-energy grain boundaries are more chemically reactive than the grains. Under certain conditions depletion or enrichment of an alloying element or impurity concentration at the grain boundaries may locally change the composition of a corrosion-resistant metal, making it susceptible to corrosive attack. Localized attack of this vulnerable region near the grain boundaries is called intergranular corrosion. In particular, the austenitic stainless steels are vulnerable to intergranular corrosion if *sensitized* by heating into the temperature range from 950° to 1450°F, which causes depletion of the chromium near the grain boundaries as chromium carbide is precipitated at the boundaries. The chromium-poor regions then corrode because of local galvanic cell action, and the grains literally fall out of the matrix. A special case of intergranular corrosion, called “weld decay,” is generated in the portion of the weld-affected zone, which is heated into the sensitizing temperature range.

To minimize the susceptibility of austenitic stainless steels to intergranular corrosion, the carbon content may be lowered to below 0.03%, stabilizers may be added to prevent depletion of the chromium near the grain boundaries, or a high-temperature solution heat treatment, called quench-annealing, may be employed to produce a more homogeneous alloy.

Other alloys susceptible to intergranular corrosion include certain aluminum alloys, magnesium alloys, copper-based alloys, and die-cast zinc alloys in unfavorable environments.

The corrosion phenomenon in which one element of a solid alloy is removed is termed selective leaching. Although the selective leaching process may occur in any of several alloy systems, the more common examples are *dezincification* of brass alloys and *graphitization* of gray cast iron. Dezincification may occur as either a highly local “plug-type” or a broadly distributed layer-type attack. In either case, the dezincified region is porous, brittle, and weak. Dezincification may be minimized by adding inhibitors such as arsenic, antimony, or phosphorous to the alloy; by lowering oxygen in the environment; or by using cathodic protection.

In the case of graphitization of gray cast iron, the environment selectively leaches the iron matrix to leave the graphite network intact to form an active galvanic cell. Corrosion then proceeds to destroy the machine part. Use of other alloys, such as nodular or malleable cast iron, mitigates the problem because there is no graphite network in these alloys to support the corrosion residue. Other alloy systems in adverse environments that may experience selective leaching include aluminum bronzes, silicon bronzes, and cobalt alloys.

Erosion corrosion is an accelerated, direct chemical attack of a metal surface due to the action of a moving corrosive medium. Because of the abrasive wear action of the moving fluid, the formation of a protective layer of corrosion product is inhibited or prevented, and the corroding medium has direct access to bare, unprotected metal. Erosion corrosion is usually characterized by a pattern of grooves or peaks and valleys generated by the flow pattern of the corrosive medium. Most alloys are susceptible to erosion corrosion, and many different types of corrosive media may induce erosion corrosion, including flowing gases, liquids, and solid aggregates. Erosion corrosion may become a problem in such machine parts as valves, pumps, blowers, turbine blades and nozzles, conveyors, and piping and ducting systems, especially in the regions of bends and elbows.

Erosion corrosion is influenced by the velocity of the flowing corrosive medium, turbulence of the flow, impingement characteristics, concentration of abrasive solids, and characteristics of the metal alloy surface exposed to the flow. Methods of minimizing or preventing erosion corrosion include reducing the velocity, eliminating or reducing turbulence, avoiding sudden changes in the direction of flow, eliminating direct impingement where possible, filtering out abrasive particles, using harder and more corrosion-resistant alloys, reducing the temperature, using appropriate surface coatings, and using cathodic protection techniques.

Cavitation often occurs in hydraulic systems, such as turbines, pumps, and piping, when pressure changes in a flowing liquid give rise to the formation and collapse of vapor bubbles at or near the containing metal surface. The impact associated with vapor bubble collapse may produce high-pressure shock waves that may plastically deform the metal locally or destroy any protective surface

film of corrosion product and locally accelerate the corrosion process. Furthermore, the tiny depressions so formed act as a nucleus for subsequent vapor bubbles, which continue to form and collapse at the same site to produce deep pits and pockmarks by the combined action of mechanical deformation and accelerated chemical corrosion. This phenomenon is called cavitation corrosion. Cavitation corrosion may be reduced or prevented by eliminating the cavitation through appropriate design changes. Smoothing the surfaces, coating the walls, using corrosion-resistant materials, minimizing pressure differences in the cycle, and using cathodic protection are design changes that may be effective.

Hydrogen damage, although not considered to be a form of direct corrosion, is often induced by corrosion. Any damage caused in a metal by the presence of hydrogen or the interaction with hydrogen is called hydrogen damage. Hydrogen damage includes hydrogen blistering, hydrogen embrittlement, hydrogen attack, and decarburization.

Hydrogen blistering is caused by the diffusion of hydrogen atoms into a void within a metallic structure where they combined to form molecular hydrogen. The hydrogen pressure builds to a high level that, in some cases, causes blistering, yielding, and rupture. Hydrogen blistering may be minimized by using materials without voids, by using corrosion inhibitors, or by using hydrogen-impervious coatings.

Hydrogen embrittlement is also caused by the penetration of hydrogen into the metallic structure to form brittle hydrides and pin dislocation movement to reduce slip, but the exact mechanism is not yet fully understood. Hydrogen embrittlement is more serious at the higher-strength levels of susceptible alloys, which include most of the high-strength steels. Reduction and prevention of hydrogen embrittlement may be accomplished by "baking out" the hydrogen at relatively low temperatures for several hours, use of corrosion inhibitors, or use of less susceptible alloys.

Decarburization and hydrogen attack are both high-temperature phenomena. At high temperatures hydrogen removes carbon from an alloy, often reducing its tensile strength and increasing its creep rate. This carbon-removing process is called *decarburization*. It is also possible that the hydrogen may lead to the formation of methane in the metal voids, which may expand to form cracks, another form of hydrogen attack. Proper selection of alloys and coatings is helpful in prevention of these corrosion-related problems.

Biological corrosion is a corrosion process or processes that results from the activity of living organisms. These organisms may be microorganisms, such as aerobic or anaerobic bacteria, or they may be macroorganisms, such as fungi, mold, algae, or barnacles. The organisms may influence or produce corrosion by virtue of their processes of food ingestion and waste elimination. There are, for example, sulfate-reducing anaerobic bacteria, which produce iron sulfide when in contact with buried steel structures, and aerobic sulfur-oxidizing bacteria, which produce localized concentrations of sulfuric acid and serious corrosive attack on buried steel and concrete pipe lines. There are also iron bacteria, which ingest ferrous iron and precipitate ferrous hydroxide to produce local crevice corrosion attack. Other bacteria oxidize ammonia to nitric acid, which attacks most metals, and most bacteria produce carbon dioxide, which may form the corrosive agent carbonic acid. Fungi and mold assimilate organic matter and produce organic acids. Simply by their presence, fungi may provide the site for crevice corrosion attacks, as does the presence of attached barnacles and algae. Prevention or minimization of biological corrosion may be accomplished by altering the environment or by using proper coatings, corrosion inhibitors, bactericides or fungicides, or cathodic protection.

### 18.9.2 Stress Corrosion Cracking

Stress corrosion cracking is an extremely important failure mode because it occurs in a wide variety of different alloys. This type of failure results from a field of cracks produced in a metal alloy under the combined influence of tensile stress and a corrosive environment. The metal alloy is not attacked over most of its surface, but a system of intergranular or transgranular cracks propagates through the matrix over a period of time.

Stress levels that produce stress corrosion cracking are well below the yield strength of the material, and residual stresses as well as applied stresses may produce failure. The lower the stress level, the longer is the time required to produce cracking, and there appears to be a threshold stress level below which stress corrosion cracking does not occur. (See p. 96 of Ref. 134.)

The chemical compositions of the environments that lead to stress corrosion cracking are highly specific and peculiar to the alloy system, and no general patterns have been observed. For example, austenitic stainless steels are susceptible to stress corrosion cracking in chloride environments but not in ammonia environments, whereas brasses are susceptible to stress corrosion cracking in ammonia environments but not in chloride environments. Thus, the "season cracking" of brass cartridge cases in the crimped zones was found to be stress corrosion cracking due to the ammonia resulting from decomposition of organic matter. Likewise, "caustic embrittlement" of steel boilers, which resulted in many explosive failures, was found to be stress corrosion cracking due to sodium hydroxide in the boiler water.

Stress corrosion cracking is influenced by stress level, alloy composition, type of environment, and temperature. Crack propagation seems to be intermittent, and the crack grows to a critical size,

after which a sudden and catastrophic failure ensues in accordance with the laws of fracture mechanics. Stress corrosion crack growth in a statically loaded machine part takes place through the interaction of mechanical strains and chemical corrosion processes at the crack tip. The largest value of plane strain stress intensity factor for which crack growth does not take place in a corrosive environment is designated  $K_{Isc}$ . In many cases, corrosion fatigue behavior is also related to the magnitude of  $K_{Isc}$ .<sup>9</sup>

Prevention of stress corrosion cracking may be attempted by lowering the stress below the critical threshold level, choice of a better alloy for the environment, changing the environment to eliminate the critical corrosive element, use of corrosion inhibitors, or use of cathodic protection. Before cathodic protection is implemented care must be taken to ensure that the phenomenon is indeed stress corrosion cracking because hydrogen embrittlement is accelerated by cathodic protection techniques.

### 18.10 FAILURE ANALYSIS AND RETROSPECTIVE DESIGN

In spite of all efforts to design and manufacture machines and structures to function properly without failure, failures do occur. Whether the failure consequences simply represent an annoying inconvenience, such as a "binding" support on the sliding patio screen, or a catastrophic loss of life and property, as in the crash of a jumbo jet, it is the responsibility of the designer to glean all of the information possible from the failure event so that similar events can be avoided in the future. Effective assessment of service failures usually requires the intense interactive scrutiny of a team of specialists, including at least a mechanical designer and a materials engineer trained in failure analysis techniques. The team might often include a manufacturing engineer and a field service engineer as well. The mission of the failure analysis team is to discover the initiating cause of failure, identify the best solution, and redesign the product to prevent future failures. Although the results of failure analysis investigations may often be closely related to product liability litigation, the legal issues will not be addressed in this discussion.

Techniques utilized in the failure analysis effort include the inspection and documentation of the event through direct examination, photographs and eyewitness reports; preservation of all parts, especially failed parts; and pertinent calculations, analyses, and examinations that may help establish and validate the cause of failure. The materials engineer may utilize macroscopic examination, low-power magnification, microscopic examination, transmission or scanning electron microscopic techniques, energy-dispersive X-ray techniques, hardness tests, spectrographic analysis, metallographic examination, or other techniques of determining the failure type, failure location, material abnormalities, and potential causes of failure. The designer may perform stress and deflection analyses, examine geometry, assess service loading and environmental influences, reexamine the kinematics and dynamics of the application, and attempt to reconstruct the failure scenario. Other team members may examine the quality of manufacture, the quality of maintenance, the possibility of unusual or unconventional usage by the operator, or other factors that may have played a role in the service failure. Piecing all of this information together, it is the objective of the failure analysis team to identify as accurately as possible the probable cause of failure.

As undesirable as service failures may be, the results of a well-executed failure analysis may be transformed directly into improved product reliability by a designer who capitalizes on service failure data and failure analysis results. These techniques of retrospective design have become important working tools of the profession and are likely to continue to grow in importance.

### REFERENCES

1. J. A. Collins, *Failure of Materials in Mechanical Design; Analysis, Prediction, Prevention*, 2nd ed., Wiley, New York, 1993.
2. "Progress in Measuring Fracture Toughness and Using Fracture Mechanics," *Materials Research and Standards*, 103-119 (March 1964).
3. H. M. Westergaard, "Bearing Pressures and Cracks," *Trans. ASME* **61**, A49 (1939).
4. G. R. Irwin, "Analysis of Stresses and Strains Near the End of a Crack Traversing a Plate," *Journal of Applied Mechanics* **24**, 361 (1957).
5. H. Tada, P. C. Paris, and G. R. Irwin, *The Stress Analysis of Cracks Handbook*, 2nd ed., Paris Productions, St. Louis, 1985.
6. T. L. Anderson, *Fracture Mechanics, Fundamentals and Applications*, 2nd ed., CRC Press, Boca Raton, FL, 1995.
7. X. Wu and A. J. Carlsson, *Weight Functions and Stress Intensity Factor Solutions*, Pergamon Press, Oxford, 1991.
8. E 399-90, "Standard Test Method for Plane-Strain Fracture Toughness of Metallic Materials," Annual Book of ASTM Standards, Vol. 03.01, American Society for Testing and Materials, Philadelphia, PA, 1991.
9. R. W. Hertzberg, *Deformation and Fracture Mechanics of Engineering Materials*, 3rd ed., Wiley, New York, 1989.

10. J. P. Gallagher (ed.), *Damage Tolerant Design Handbook*, 4 Vols., Metals and Ceramics Information Center, Battelle Columbus Labs., Columbus, OH, 1983.
11. *Metallic Materials and Elements for Aerospace Vehicle Structures*, MIL-HDBK-5F, 2 Vols., U. S. Dept. of Defense, Naval Publications and Forms Center, Philadelphia, PA, 1987.
12. W. T. Matthews, *Plane Strain Fracture Toughness ( $K_{IC}$ ) Data Handbook for Metals*, Report No. AMMRC MS 73-6, U. S. Army Materiel Command, NTIS, Springfield, VA, 1973.
13. C. M. Hudson and S. K. Seward, "A Compendium of Sources of Fracture Toughness and Fatigue Crack Growth Data for Metallic Alloys," *International Journal of Fracture* **14**, R151 (1978).
14. C. M. Hudson and S. K. Seward, "A Compendium of Sources of Fracture Toughness and Fatigue Crack Growth Data for Metallic Alloys-Part II," *International Journal of Fracture* **20**, R59 (1982).
15. C. M. Hudson and S. K. Seward, "A Compendium of Sources of Fracture Toughness and Fatigue Crack Growth Data for Metallic Alloys-Part III," *International Journal of Fracture* **39**, R43 (1989).
16. C. M. Hudson and J. J. Ferrainolo, "A Compendium of Sources of Fracture Toughness and Fatigue Crack Growth Data for Metallic Alloys-Part IV," *International Journal of Fracture* **48**, R19 (1991).
17. G. R. Irwin, "Fracture Mode Transition for a Crack Traversing a Plate," *Journal of Basic Engineering* **82**, 417 (1960).
18. M. F. Kanninen and C. H. Popelar, *Advanced Fracture Mechanics*, Oxford University Press, New York, 1985.
19. D. Broek, *Elementary Engineering Fracture Mechanics*, 4th ed., Kluwer, London, 1986.
20. G. C. Sih, *Handbook of Stress Intensity Factors for Researchers and Engineers*, Institute of Fracture and Solid Mechanics, Lehigh University, Bethlehem, PA, 1973.
21. D. P. Rooke and D. J. Cartwright, *Compendium of Stress Intensity Factors*, Her Majesty's Stationery Office, London, 1976.
22. J. M. Barsom and S. T. Rolfe *Fracture and Fatigue Control in Structures*, 2nd ed., Prentice-Hall, Englewood Cliffs, NJ, 1987.
23. A. P. Parker, *The Mechanics of Fracture and Fatigue*, E. & F. N. Spon Ltd., New York, 1981.
24. R. P. Harrison, K. Loosemore, and I. Milne, "Assessment of the Integrity of Structures Containing Cracks," CEGB Report R/H/R6, Central Electricity Generating Board, United Kingdom (1976).
25. A. G. Miller, "Review of Limit Loads of Structures Containing Defects," *International Journal of Pressure Vessels and Piping* **32**, 197 (1988).
26. H. J. Grover, S. A. Gordon, and L. R. Jackson, *Fatigue of Metals and Structures*, Government Printing Office, Washington, DC, 1954.
27. A. Higdon, E. H. Ohlsen, W. B. Stiles, J. A. Weese, and W. F. Riley, *Mechanics of Materials*, 4th ed., Wiley, New York, 1985.
28. W. M. Murray (ed.), *Symposium on Fatigue and Fracture of Metals*, Wiley, New York, 1952.
29. J. B. Johnson, "Aircraft Engine Material," *SAE Journal* **40**, 153-162 (1937).
30. *Proceedings of the Conference on Welded Structures*, The Welding Institute, Cambridge, England, 1971, Vols. I and II.
31. A. F. Madayag, *Metal Fatigue, Theory and Design*, Wiley, New York, 1969.
32. H. F. Moore, "A Study of Size Effect and Notch Sensitivity in Fatigue Tests of Steel," *ASTM Proceedings* **45**, 507 (1945).
33. W. N. Thomas, "Effect of Scratches and Various Workshop Finishes Upon the Fatigue Strength of Steel," *Engineering* **116**, 449ff (1923).
34. G. V. Smith, *Properties of Metals at Elevated Temperatures*, McGraw-Hill, New York, 1950.
35. H. J. Gough and D. G. Sopwith, *Journal of Iron and Steel Institute* **127**, 301 (1933).
36. O. J. Horgor, *Metals Engineering Design* (ASME Handbook), American Society of Mechanical Engineers, McGraw-Hill, New York, 1953.
37. *Proceedings of International Conference on Fatigue*, American Society of Mechanical Engineers (jointly with Institution of Mechanical Engineers), New York, 1956.
38. N. E. Frost and K. Denton, "The Fatigue Strength of Butt Welded Joints in Low Alloy Structural Steels," *British Welding Journal* **14**(4) (1967).
39. F. M. Howell and J. L. Miller, "Axial Stress Fatigue Strengths of Several Structural Aluminum Alloys," *ASTM Proceedings* **55**, 955 (1955).

40. Battelle Memorial Institute, *Prevention of Fatigue in Metals*, Wiley, New York, 1941.
41. H. J. Grover, *Fatigue of Aircraft Structures*, Government Printing Office, Washington, DC, 1966.
42. J. A. Bannantine, J. J. Comer, and J. L. Handrock, *Fundamentals of Metal Fatigue Analysis*, Prentice-Hall, Englewood Cliffs, NJ, 1990.
43. S. Suresh, *Fatigue of Materials*, Cambridge University Press, 1991.
44. N. E. Dowling, *Mechanical Behavior of Materials*, Prentice-Hall, Englewood Cliffs, NJ, 1993.
45. H. O. Fuchs and R. I. Stephens, *Metal Fatigue in Engineering*, Wiley, New York, 1980.
46. R. E. Peterson, *Stress Concentration Factors*, Wiley, New York, 1974.
47. E. Z. Stowell, "Stress and Strain Concentration at a Circular Hole in an Infinite Plate," NACA TN2073, National Advisory Committee for Aeronautics, Cleveland, OH, April 1950.
48. G. Sines and J. L. Waisman, *Metal Fatigue*, McGraw-Hill, New York, 1959.
49. R. C. Juvinall, *Engineering Considerations of Stress, Strain, and Strength*, McGraw-Hill, New York, 1967.
50. *Manual on Low Cycle Fatigue Testing*, STP 465, American Society for Testing and Materials, Philadelphia, PA, 1969.
51. J. F. Tavernelli and L. F. Coffin, Jr., "A Compilation and Interpretation of Cyclic Strain Fatigue Tests on Metals," *ASM Transactions of American Society for Metals* **51**, 438–453 (1959).
52. S. S. Manson, "Behavior of Materials Under Conditions of Thermal Stress," NACA TN-2933, National Advisory Committee for Aeronautics, Cleveland, OH, 1954.
53. L. F. Coffin, Jr., "Design Aspects of High Temperature Fatigue with Particular Reference to Thermal Stresses," *ASME Transactions* **78**, 527–532 (1955).
54. J. Morrow, J. F. Martin, and N. E. Dowling, "Local Stress–Strain Approach to Cumulative Fatigue Damage Analysis," Final Report, T. & A. M. Report No. 379, Department of Theoretical and Applied Mechanics, University of Illinois, Urbana, IL, January 1974.
55. R. W. Landgraf, "The Resistance of Metal to Cyclic Deformation," *Achievement of High Fatigue Resistance in Metals Alloys*, STP-467, American Society for Testing and Materials, Philadelphia, PA, 1970.
56. B. M. Wundt, *Effects of Notches on Low Cycle Fatigue*, STP-490, American Society for Testing and Materials, Philadelphia, PA, 1972.
57. E. Krempl, *The Influence of State of Stress on Low-Cycle Fatigue of Structural Materials: A Literature Survey and Interpretation Report*, STP-549, American Society for Testing and Materials, Philadelphia, PA, 1974.
58. S. S. Manson, *Thermal Stress and Low Cycle Fatigue*, McGraw-Hill, New York, 1966.
59. S. J. Stadnick and J. Morrow, "Techniques for Smooth Specimen Simulation of the Fatigue Behavior of Notched Members," *Testing for Prediction of Material Performance in Structures and Components*, STP-515, American Society for Testing and Materials, Philadelphia, PA, 1972.
60. J. F. Martin, T. H. Topper, and G. M. Sinclair, "Computer Based Simulation of Cyclic Stress–Strain Behavior with Applications to Fatigue," *Materials Research and Standards* **11**(2), 23 (February 1971).
61. R. C. Rice (ed.), *Fatigue Design Handbook*, 2nd ed., SAE Pub. No. AE-10, Society of Automotive Engineers, Warrendale, PA, 1988.
62. T. H. Topper, R. M. Wetzel, and J. Morrow, "Neuber's Rule Applied to Fatigue of Notched Specimens," *Journal of Materials* **4**(1), 200–209 (1969).
63. N. E. Dowling, "Fatigue Failure Predictions for Complicated Stress-Strain Histories," *Journal of Materials* **7** (1), 71–87 (1972).
64. E 647-88a, "Standard Test Method for Measurement of Fatigue Crack Growth Rates," American Society for Testing and Materials, Philadelphia, PA, 1988.
65. J. Schijve, "Four Lectures on Fatigue Crack Growth," *Engineering Fracture Mechanics* **11**, 167–221 (1979).
66. P. C. Paris and F. Erdogan, "A Critical Analysis of Crack Propagation Laws," *Trans. ASME, Journal of Basic Engineering* **85**, 528–534 (1963).
67. S. J. Maddox, *Fatigue Strength of Welded Structures*, 2nd ed., Abington, 1991.
68. W. G. Reuter, J. H. Underwood, and J. C. Newman (eds.), *Surface-Crack Growth: Models, Experiments and Structures*, STP-1060, American Society for Testing and Materials, Philadelphia, PA, 1990.
69. W. Elber, *Eng. Fracture Mech.* **2**, 37–45 (1970).
70. J. C. Newman and W. Elber (eds.), *Mechanics of Fatigue Crack Closure*, STP-982, American Society for Testing and Materials, Philadelphia, PA, 1988.

71. L. P. Pook, *The Role of Crack Growth in Metal Fatigue*, The Metals Society, London, 1983.
72. R. D. Ritchie and J. Lankford (eds.), *Small Fatigue Cracks*, The Metallurgical Society, Inc., 1986.
73. W. G. Clark, Jr., "Fracture Mechanics in Fatigue," *Experimental Mechanics* (September 1971).
74. H. A. Wood, "Fracture Control Procedures for Aircraft Structural Integrity," AFFDL Report TR-21-89, Wright-Patterson Air Force Base, OH, July 1971.
75. F. R. Larson and J. Miller, "Time-Temperature Relationships for Rupture and Creep Stresses," *ASME Transactions* **74**, 765 (1952).
76. S. S. Manson and A. M. Haferd, "A Linear Time-Temperature Relation for Extrapolation of Creep and Stress Rupture Data," NACA Technical Note 2890, National Advisory Committee for Aeronautics, Cleveland, OH, March 1953.
77. R. G. Sturm, C. Dumont, and F. M. Howell, "A Method of Analyzing Creep Data," *ASME Transactions* **58**, A62 (1936).
78. N. H. Polakowski and E. J. Ripling, *Strength and Structure of Engineering Materials*. Prentice-Hall, Englewood Cliffs, NJ, 1966.
79. E. L. Robinson, "Effect of Temperature Variation on the Long-Time Rupture Strength of Steels," *ASME Transactions* **74**, 777-781 (1952).
80. A. J. Kennedy, *Processes of Creep and Fatigue in Metals*, Wiley, New York, 1963.
81. F. W. Demoney and B. J. Lazan, WADC Tech Report 53-510, Wright-Patterson Air Force Base, OH, 1954.
82. F. Vitovec and B. J. Lazan, *Symposium on Metallic Materials for Service at Temperatures Above 1600°F*, STP-174, American Society for Testing and Materials, Philadelphia, PA, 1956.
83. L. F. Coffin, Jr., "The Effect of Frequency on the Cyclic Strain and Low Cycle Fatigue Behavior of Cast Udimet 500 at Elevated Temperature," *Metallurgical Transactions* **12**, 3105-3113 (November 1971).
84. J. B. Conway and J. T. Berling, "A New Correlation of Low-Cycle Fatigue Data Involving Hold Periods," *Metallurgical Transactions* **1**(1), 324-325 (January 1970).
85. J. R. Ellis and E. P. Esztergar, "Considerations of Creep-Fatigue Interaction in Design Analysis," *Symposium on Design for Elevated Temperature Environment*, ASME, New York, 1971, pp. 29-33.
86. R. M. Curran and B. M. Wundt, "A Program to Study Low-Cycle Fatigue and Creep Interaction in Steels at Elevated Temperatures," *Current Evaluation of 2 1/4 Chrome 1 Molybdenum Steel in Pressure Vessels and Piping*, ASME, New York, 1972, pp. 49-82.
87. S. S. Manson, G. R. Halford, and M. H. Hirschberg, "Creep-Fatigue Analysis by Strain-Range Partitioning," *Symposium on Design for Elevated Temperature Environment*, ASME, New York, 1971, pp. 12-24.
88. M. M. Leven, "The Interaction of Creep and Fatigue for a Rotor Steel," *Experimental Mechanics* **13**(9), 353-372 (September 1973).
89. S. S. Manson, G. R. Halford, and M. H. Hirschberg, NASA Technical Memo TMX-67838, Lewis Research Center, Cleveland, OH, May 1971.
90. J. F. Saltzman and G. R. Halford, "Application of Strain-Range Partitioning to the Prediction of Creep-Fatigue Lives of AISI Types 304 and 316 Stainless Steel," NASA Technical Memo TMX-71898, Lewis Research Center, Cleveland, OH, September 1976.
91. C. G. Annis, M. C. Van Wanderham, and R. M. Wallace, "Strain-Range Partitioning Behavior of an Automotive Turbine Alloy," Final Report NASA TR 134974, February 1976.
92. M. H. Hirschberg and G. R. Halford, "Use of Strain-Range Partitioning to Predict High-Temperature Low Cycle Fatigue Life," NASA TN D-8072, January 1976.
93. J. F. Saltzman and G. R. Halford, "Application of Strain-Range Partitioning to the Prediction of MPC Creep-Fatigue Data for 2 1/4 Cr-1 Mo Steel," NASA TMX-73474, December 1976.
94. S. S. Manson and G. R. Halford, "Treatment of Multiaxial Creep-Fatigue by Strain-Range Partitioning," NASA TMX-73488, December 1976.
95. *Characterization of Low Cycle High Temperature Fatigue by the Strain-Range Partitioning Method*, AGARD Conference Proceedings No. 243, distributed by NASA, Langley Field, VA, April 1978.
96. J. A. Collins, "Fretting-Fatigue Damage-Factor Determination," *Journal of Engineering for Industry* **87**(8), 298-302 (August 1965).
97. D. Godfrey, "Investigation of Fretting by Microscopic Observation," NACA Report 1009, Cleveland, OH, 1951 (formerly TN-2039, February 1950).

98. F. P. Bowden and D. Tabor, *The Friction and Lubrication of Solids*, Oxford University Press, Amen House, London, 1950.
99. D. Godfrey and J. M. Baily, "Coefficient of Friction and Damage to Contact Area During the Early Stages of Fretting; I—Glass, Copper, or Steel Against Copper," NACA TN-3011, Cleveland, OH, September 1953.
100. M. E. Merchant, "The Mechanism of Static Friction," *Journal of Applied Physics* **11**(3), 232 (1940).
101. E. E. Bisson, R. L. Johnson, M. A. Swikert, and D. Godfrey, "Friction, Wear, and Surface Damage of Metals as Affected by Solid Surface Films," NACA TN-3444, Cleveland, OH, May 1955.
102. H. H. Uhlig, "Mechanisms of Fretting Corrosion," *Journal of Applied Mechanics* **76**, 401–407 (1954).
103. I. M. Feng and B. G. Rightmire, "The Mechanism of Fretting," *Lubrication Engineering* **9**, 134ff (June 1953).
104. I. M. Feng, "Fundamental Study of the Mechanism of Fretting," Final Report. Lubrication Laboratory, Massachusetts Institute of Technology, Cambridge, 1955.
105. H. T. Corten, "Factors Influencing Fretting Fatigue Strength," T. & A. M. Report No. 88, Department of Theoretical and Applied Mechanics, University of Illinois, Urbana, IL, June 1955.
106. W. L. Starkey, S. M. Marco, and J. A. Collins, "Effects of Fretting on Fatigue Characteristics of Titanium–Steel and Steel–Steel Joints," ASME Paper 57-A-113, New York, 1957.
107. W. D. Milestone, "Fretting and Fretting-Fatigue in Metal-to-Metal Contacts," ASME Paper 71-DE-38, New York, 1971.
108. G. P. Wright and J. J. O'Connor, "The Influence of Fretting and Geometric Stress Concentrations on the Fatigue Strength of Clamped Joints," *Proceedings, Institution of Mechanical Engineers*, 186 (1972).
109. R. B. Waterhouse, *Fretting Corrosion*, Pergamon Press, New York, 1972.
110. "Fretting in Aircraft Systems," AGARD Conference Proceedings CP161, distributed through NASA, Langley Field, VA, 1974.
111. "Control of Fretting Fatigue," Report No. NMAB-333, National Academy of Sciences, National Materials Advisory Board, Washington, DC, 1977.
112. N. P. Suh, S. Jahanmir, J. Fleming, and E. P. Abrahamson, "The Delamination Theory of Wear—II," Progress Report, Materials Processing Lab, Mechanical Engineering Dept., MIT Press, Cambridge, MA, September 1975.
113. J. T. Burwell, Jr., "Survey of Possible Wear Mechanisms," *Wear* **1**, 119–141 (1957).
114. M. B. Peterson, M. K. Gabel, and M. J. Derine, "Understanding Wear"; K. C. Ludema, "A Perspective on Wear Models"; E. Rabinowicz, "The Physics and Chemistry of Surfaces"; J. McGrew, "Design for Wear of Sliding Bearings"; R. G. Bayer, "Design for Wear of Lightly Loaded Surfaces," *ASTM Standardization News* **2**(9), 9–32 (September 1974).
115. R. B. Waterhouse, *Fretting Corrosion*, Pergamon Press, New York, 1972.
116. P. A. Engel, "Predicting Impact Wear," *Machine Design*, 100–105 (May 1977).
117. P. A. Engel, *Impact Wear of Materials*, Elsevier, New York, 1976.
118. J. A. Collins, "A Study of the Phenomenon of Fretting-Fatigue with Emphasis on Stress-Field Effects," Dissertation, Ohio State University, Columbus, 1963.
119. J. A. Collins and F. M. Tovey, "Fretting Fatigue Mechanisms and the Effect of Direction of Fretting Motion on Fatigue Strength," *Journal of Materials* **7**(4) (December 1972).
120. W. D. Milestone, "An Investigation of the Basic Mechanism of Mechanical Fretting and Fretting-Fatigue at Metal-to-Metal Joints, with Emphasis on the Effects of Friction and Friction-Induced Stresses," Dissertation, Ohio State University, Columbus, 1966.
121. J. A. Collins and S. M. Marco, "The Effect of Stress Direction During Fretting on Subsequent Fatigue Life," *ASTM Proceedings* **64**, 547 (1964).
122. J. A. Alic, "Fretting Fatigue in the Presence of Periodic High Tensile or Compressive Loads," Final Scientific Report, Grant No. AFOSR77-3422, Wright-Patterson AFB, Ohio, April 1979.
123. H. Lyons, "An Investigation of the Phenomenon of Fretting-Wear and Attendant Parametric Effects Towards Development of Failure Prediction Criteria," Ph.D. Dissertation, Ohio State University, Columbus, 1978.
124. P. L. Ko, "Experimental Studies of Tube Fretting in Steam Generators and Heat Exchangers," ASME/CSME Pressure Vessels and Piping Conference, Nuclear and Materials Division, Montreal, Canada, June 1978.

125. R. B. Heywood, *Designing Against Fatigue of Metals*, Reinhold, New York, 1962.
126. F. P. Bowden and D. Tabor, *Friction and Lubrication of Solids*, Oxford University Press, London, 1950.
127. F. P. Bowden and D. Tabor, *Friction and Lubrication*, Methuen, London, 1967.
128. E. Rabinowicz, *Friction and Wear of Materials*, Wiley, New York, 1966.
129. C. Lipson, *Wear Considerations in Design*, Prentice-Hall, Englewood Cliffs, NJ, 1967.
130. N. P. Suh, "The Delamination Theory of Wear," *Wear* **25**, 111–124 (1973).
131. J. E. Shigley, *Mechanical Engineering Design*, 2nd ed., McGraw-Hill, New York, 1972.
132. W. A. Glaeser, K. C. Ludema, and J. K. Rhee (eds.), *Wear Materials*, American Society of Mechanical Engineers, New York, April 25–28, 1977.
133. C. W. MacGregor (ed.), *Handbook of Analytical Design for Wear*, Plenum Press, New York, 1964.
134. M. G. Fontana and N. D. Greene, *Corrosion Engineering*, McGraw-Hill, New York, 1967.
135. L. S. Seabright and R. J. Fabian, "The Many Faces of Corrosion," *Materials in Design Engineering* **57**(1) (January 1963).
136. G. Nelson, *Corrosion Data Survey*, National Association of Corrosion Engineers, Houston, TX, 1972.
137. H. H. Uhlig (ed.), *Corrosion Handbook*, Wiley, New York, 1948.
138. E. Rabald, *Corrosion Guide*, Elsevier, New York, 1951.